



MEDRC Series of R & D Reports
MEDRC Project: 14-JS-032

Synthesis of fouling-resistant ultrafiltration membranes from nanosturctured composites for water treatment applications

MSc. Thesis By

Sukaina Sulaiman Al-ratrout

Supervisors

Dr. Yazan Ahed Hussain

Thesis submitted in partial fulfillment of the requirements for the degree of
M.Sc. in chemical engineering

**The Middle East Desalination Research Center
Muscat
Sultanate of Oman**

August 2015

SYNTHESIS OF FOULING-RESISTANT ULTRAFILTRATION MEMBRANES FROM NANOSTRUCTURED COMPOSITES FOR WATER TREATMENT APPLICATIONS

By

Sukaina Sulaiman Al-ratrout

Dr. Yazan Ahed Hussain

Thesis submitted in partial fulfillment of the requirements for the degree of
M.Sc. in chemical engineering

At

The Faculty of Graduate Studies

Jordan University of Science and Technology

August, 2015

SYNTHESIS OF FOULING-RESISTANT ULTRAFILTRATION MEMBRANES FROM NANOSTRUCTURED COMPOSITES FOR WATER TREATMENT APPLICATIONS

By

Sukaina Sulaiman Al-ratrout

Signature of Author

.....

Committee Member

Signature and Date

Dr. Yazan A. Hussain (Chairman)

.....

Dr. Mohamad Al-Saleh (Member)

.....

Dr. Abeer Albsoul (External Examiner)

.....

August, 2015

تفويض

نحن الموقعين أدناه، نتعهد بمنح جامعة العلوم والتكنولوجيا الاردنية حرية التصرف في نشر محتوى الرسالة الجامعية، بحيث تعود حقوق الملكية الفكرية لرسالة الماجستير الى الجامعة وفق القوانين والانظمة والتعليمات المتعلقة بالملكية الفكرية وبراءة الاختراع.

المشرف الرئيس (ثلاثة مقاطع)	الطالبة (ثلاثة مقاطع)
د. يزن عاهد حسين	سكينة سليمان الرطروط
التوقيع و التاريخ	الرقم الجامعي و التوقيع
.....	20133022003

Dedication

I would like to dedicate this thesis to my family. My parents Suliman and Randa for being my biggest fans. For their endless love and support and for so much more. To my future husband Ali, who heard every thought and who was there at every struggle during these past two years. And to my brothers Jihad, Omar and Hamza the funniest most amazing brothers in the world. I love you and I am forever blessed and grateful to have you all in my life. You are the best people in the whole world and I dedicate this modest work in your honor.

Acknowledgments

During the past year, I was inspired, encouraged, helped and motivated by a lot of people. They contributed in the construction of this thesis in one way or the other. One person stands out the most because he was there reading every draft, editing every thought and helping me construct a better experimental protocols. Namely, Dr. Yazan Hussain, it is a cliché to say I would like to express my deepest gratitude to my supervisor. In my case, my deepest gratitude is not even enough. Dr. Yazan was more than just a supervisor, he believed in me when I didn't even believe in myself. He was supportive, critical and respectful towards me and my research. He taught me how to write and how criticize my own work. He taught me the basics of research, the most interesting parts of it. Dr. Yazan, from the bottom of my heart I thank you.

I would like to thank my mom and dad. They are the best parents any child could dream of. During my whole life you have supported every decision I made with the purpose of making me happy. I love you with all my heart and I wish I could be as supportive and as loving as you are. I would like to thank my future husband Ali. The most interesting person I have ever met. You make me see things through a lens of reason. Thank you for always reminding to use “think” instead of “feel” when writing. Thank you for always being there for me, always listening and always making my day. Ali, you are beyond amazing. Thank you.

To my brother Jehad, Omar and Hamza you are wonderful and I love you. Thank you Jehad because you were always nice to me. Omar for making me laugh and Hamza for being the sweetest most amazing little brother and friend any girl could ever wish for.

I would also like to thank my family in-law. My father in law Saleh Akl and my mother in law Mahasen Aoun for their beautiful encouraging words and for their prayers. I would like to thank Fadi Akl and Mohammad Akl my brothers in law for being a great brothers

in law. I would like my cousins and my uncles and aunts for always asking how things were going. For trying to be polite and listening to me when I start talking about my thesis. I would like to thank you for all your prayers and love. Specially, Uncle Zakarya, aunt Taghreed, Uncle Ibrahim and Aunt Suzan. Thank you very much for all your love and prayers.

I would like to thank my friends. Smr Mahmood, Jomana Nuirat, Raneem Faisal, Safaa Dannoon, Walaa Saadeh, Eman Saadeh, Eman Zaki, Israa Hammori, Hiba Abu Zaghley and Hadeel Saqlawi. Thank you for all your support and love. Thank you for all the tea and all the coffee. Thank you for always praying for me and pushing me forward.

Finally, I would like to thank the faculty members of the chemical engineering department. Specially Dr. Mohammad Al-Saleh for his helpful comments and thoughts along the way. And for teaching me the basics of mass transfer and the beauty of equations and models. I would also like to thank Dr. Khaleel Al-Halhooli, Dr. Nehal Abu Lail, Dr. Khaled Hatamleh, Dr. Ziad Al-Ghzawi, and Dr. Abdulrahman Al-Tamimi for all their hard work and helpful insight into what it takes to be a good researcher. I would like to thank the rest of the chemical engineering department faculty, Dr. Majdi Mahasneh, Dr. Mohammad Azzam, Dr. Rami Jumah, and Dr. Fahmi Abu Al-Rub.

This thesis was financially supported by the Middle East desalination center “MEDRC”. I would love to extend my deepest gratitude to MEDRC team. I would also like to thank the deanship of research in JUST for their support.

Table of Contents

Dedication	I
Acknowledgments.....	II
Table of Contents	IV
Table of Figures	VII
Table of tables.....	X
Abstract	XII
Chapter 1: Introduction	1
Chapter 2: Literature Review	4
2.1 Membranes	4
2.2 Membrane Fabrication	7
2.2.1 Phase Inversion	8
2.2.2 Interfacial Polymerization.....	13
2.2.3 Solution Coating	14
2.2 Membrane Fouling	15
2.3 Membrane Modification	18
2.3.1 Blending Method.....	20
2.3.2 Fabrication of nanocomposite membranes.....	23
Chapter 3 Materials and Methods	34
3.1 Materials.....	34
3.2 Preparation of Membranes	34
3.2.1 Preparation of Polysulfone Membranes	34
3.2.2 Preparation of Nanocomposite Polysulfone Membranes	35
3.3 Membranes Characterization and Analysis.....	35
3.3.1 Scanning Electron Microscopy	35
3.4 Filtration Studies	35
3.5 Static Adsorption.....	37
3.6 Membrane Pore Size, Porosity and Number of Pores.....	37
Chapter 4: Effect of ZnO nanoparticles as additive on the performance and formation of polysulfone membranes fabricated via phase inversion.....	39
4.1 Results and Discussion.....	40
4.1.1 Pure Water Permeation	40
4.1.2 Membrane surface morphology and structure.....	42
4.1.3 Compaction of Membranes	45
4.1.4 Fouling and cleanability	48

4.2 Conclusions	52
Chapter 5: Effect of Tio2 Nanoparticles As Additive on the Performance and Formation of Polysulfone Membranes Fabricated Via Phase Inversion.....	54
5.1 Results and Discussion.....	55
5.1.1 Pure Water Permeability	55
5.1.2 Membranes surface morphology and structure	56
5.1.3 Compaction of membranes	59
5.1.2 Fouling and cleanability	63
5.2 Conclusions	67
Chapter 6: Summary and Future Work	70
6.1 Fabrication and performance of ZnO-nanocomposite membranes: A summary	71
6.2 Fabrication and performance of TiO ₂ -nanocomposite membranes: A summary.....	72
6.3 Recommendations for future work	72
References	74
Appendices	86
Appendix A: UV-Vis spectrum.....	86
Appendix B: Pore size and pore size distribution graphical representation.....	87
Arabic Abstract.....	92

Table of Figures

Figure 1: Schematic sketch of membrane separation (7).....	4
Figure 2: Membranes Used to Achieve Good Separation of Different Solutes. i.e. RO is Used to Remove Salts, While UF is Used to Remove Viruses (8).	5
Figure 3. A schematic sketch of symmetrical and asymmetrical membranes (4).....	6
Figure 4 SEM cross section of asymmetric Poly(vinylidene fluoride) membrane. The top layer (active layer) has finger-like structure and the sub-layer has a sponge like structure (5).	7
Figure 5. Schematic depiction of the immersion precipitation process (21).	10
Figure 6. The ternary phase inversion system and the membrane formation mechanism (25).	11
Figure 7 The membrane formation pathways based on different solvent non-solvent exchange rates and the final membrane structure obtained following each pathway (28). 12	
Figure 8 TEM images of TFC of commercial RO membrane (ESPA3). The structure of the thin polyamide (PA) layer is highly non-uniform. The polysulfone sublayer shows the presence of large pores (32).	14
Figure 9. Flux decay due to membrane fouling and restoration of flux by cleaning (4). ...	16
Figure 10. Different blocking mechanisms of colloidal particles: a) pore blocking, b) pore restriction (scaling), c) intermediate fouling, and d) cake filtration (46).....	17
Figure 11. SEM images of PS membranes prepared with: a) no PVP, and b) 7.5 wt% PVP in the cast solution (12).	20
Figure 12. Pure water flux of PNAi-PVP-modified PS membranes (17).	21
Figure 13. Pure water permeability of PS membranes containing different PANiEB concentrations (16).....	22
Figure 14. SEM images of cross sections of PS membranes modified with PEG and CCNP: a) 0:0, b) 0:5, c) 1:5, d) 2:5, e) 5:5, and f) 10 CCNP:5 PEG (wt%) (14).	24
Figure 15. Compaction behavior of bare PS membranes and 1wt%xGNPs-AuNP composite membranes (26).	26
Figure 16. SEM images of cross sections of bare and composite (with xGnP) PS membranes. Also shown is a schematic sketch of the membrane macrovoids formation in the sublayer as a function of xGnP content in the cast solution (26).	26
Figure 17 Flux of PS/TiO ₂ nanocomposite membranes during activated sludge filtration (83).....	29
Figure 18. fouling recovery ratio and BSA rejection of PS membrane modified with different ratios of TiO ₂ /PANi (M0: 0, M1: 0.05, M2: 0.1, M3: 1.0, and M4: 1.5 wt%) (72).	31
Figure 19 pure water flux of ZnO-nanocomposite membranes with different ZnO concentrations in the casting solution. Each line presents the average of four samples. Membranes were tested using distilled water at 3 bar.	41
Figure 20 Pure water flux of ZnO-nanocomposite membranes with different ZnO concentrations in the casting solution. Membranes were tested using distilled water at 3 bar. Each bar represents the average of four samples	41
Figure 21. SEM images of cross sections of membranes with different ZnO concentrations in the casting solution: (a) PS, (b) 1% ZnO, (c) 2% ZnO, (d) 4% ZnO.....	44

Figure 22 Effect of different ZnO concentrations on the flux loss of nanocomposite membranes. Flux was measured using distilled water at 5 bar. Each bar represents the average of 4 samples.	46
Figure 23. Effect of ZnO concentrations on -compaction exponent nanocomposite membranes. Membranes were tested for 1 hour using deionized water at 5 bar. Each point represents the average of 4samples.	47
Figure 24. TEM images of different membranes: (a) PS, (b) 2% ZnO (c) and (d) 4% ZnO. Scale bars are 500 nm.	48
Figure 25. Effect of ZnO concentration on flux during HA filtration. Membranes were tested using 15 ppm HA at 3 bar. Each curve represents an average of 4 membrane samples.	49
Figure 26. Appearance of different membranes after HA fouling experiments.	49
Figure 27 Effect of different concentrations of ZnO-nanocomposite membranes on percentage of weight increase during static adsorption test. Static adsorption test was carried out using 15 ppm HA at room temperature.	51
Figure 28. Flux recovery ration for different HA-fouled membranes. Membranes were tested using deionized water at 3 bar and no stirring. Each bar represents the average of at least 2 samples.	52
Figure 29 pure water flux of TiO ₂ -nanocomposite membranes with different TiO ₂ concentrations in the casting solution. Each line presents the average of four samples. Membranes were tested using distilled water at 3 bar.	55
Figure 30. Effect of TiO ₂ concentration on pure water permeation. PWP was measured using distilled water at 3 bars. Each bar represents the average of 4samples.	56
Figure 31. SEM images of cross sections of TiO ₂ -nanocomposite membranes: (a) PS (b) 2% TiO ₂ and (c) 4% TiO ₂ in the casting solution.	58
Figure 32. Effect of TiO ₂ concentration on flux loss during compaction at 5 bars. Flux was measured using distilled water at 5 bar. Each bar represents the average of 4 samples.	59
Figure 33 Effect of different TiO ₂ concentrations in membranes on pre-compaction exponent factor and scatter for PS- TiO ₂ nanocomposite membranes, each point is averaged over four samples.	61
Figure 34 TEM images of different membrane samples at PS, 2% TiO ₂ and 4% TiO ₂ concentration.	62
Figure 35 Effect of ZnO concentration on flux during HA filtration. Membranes were tested using 15 ppm HA at 3 bar. Each curve represents an average of 4 membrane samples.	63
Figure 36. Effect of TiO ₂ concentration on the relative flux during HA filtration. Each curve represents an average of 4 samples.	64
Figure 37 effect of TiO ₂ in the membrane on the percentage of weight increase during static adsorption test.	65
Figure 38. Effect of TiO ₂ concentration on HA rejection. Each bar represents the average of 4 samples.	66
Figure 39 Appearance of different membranes after HA fouling experiments a) PS, b) 1% TiO ₂ nanocomposite membranes, c) 4% TiO ₂ nanocomposite membranes	67
Figure 40 Concentration and absorbance of humic acid using UV-vis at λ 283 nm.	86

Figure 41 Solute separation curve of polysulfone. The rejection is plotted against $\log(d)$, where d is the diameter of PEG used in the solution	87
Figure 42 Solute separation curve of 1% TiO_2 . The rejection is plotted against $\log(d)$, where d is the diameter of PEG used in the solution.	88
Figure 43 Solute separation curve of 4% TiO_2 . The rejection is plotted against $\log(d)$, where d is the diameter of PEG used in the solution.	88
Figure 44 Solute separation curve of 1% ZnO . The rejection is plotted against $\log(d)$, where d is the diameter of PEG used in the solution.	89
Figure 45 Solute separation curve of 4% ZnO . The rejection is plotted against $\log(d)$, where d is the diameter of PEG used in the solution	89
Figure 46 Pore size distribution of polysulfone (0%) membranes.....	90
Figure 47 Pore distribution of 1% and 4% ZnO membranes.....	90
Figure 48 Pore distribution of 1% and 4% TiO_2 membranes.....	91

Table of tables

Table 1 The most commonly used polymers in phase inversion (immersion precipitation), their advantages and disadvantages	9
Table 2. The Parameters Effecting Rate of Fouling by NOM.	18
Table 3 porosity (ϵ), mean pore diameter (μp), and geometric standard deviation (σp) of ZnO nanocomposite membranes.....	42
Table 4 porosity (ϵ), mean pore diameter (μp), and geometric standard deviation (σp) of TiO ₂ nanocomposite membranes.....	70

Table of Appendices

Appendix A: UV-Vis spectrum.....	86
Appendix B: Pore size and pore size distribution graphical representation	Error! Bookmark not defined.

Abstract

Synthesis of Fouling-Resistant Ultrafiltration Membranes From Nanosturctured Composites For Water Treatment Applications

By

Sukaina Sulaiman Al-ratrout

Membranes became an integral part of water treatment facilities. Despite their numerous advantages, membranes suffer from a major drawback namely fouling. Nanomaterials have been previously used to modify membranes structure aiming to fabricate anti-fouling membranes. The role of zinc oxide (ZnO) nanoparticles and titanium dioxide (TiO₂) nanoparticles (NP's) in natural organic matter (NOM) fouling of nanocomposite ultrafiltration membranes is investigated. These nanoparticles were chosen because they have been systemically studied in literature.

Results of fouling experiments using humic acid showed ZnO-nanocomposite membranes had a higher affinity to be fouled compared to virgin polysulfone membranes. There are several reasons for the aggravated fouling noted for ZnO-nanocomposite membranes. The higher permeation drag of ZnO-nanocomposite membranes combined with large surface area of ZnO NP's, which allows ligand exchange to take place between the phenolic COOH and OH groups in humic acid and ZnO NP's surface. Add to that the release of Zn⁺² cations from ZnO NP's, which has a prominent effect on the exacerbation of fouling of membranes. On the other hand, TiO₂-nanocomposite membranes had an improved anti-fouling properties compared to both virgin polysulfone and ZnO-nanocomposite membranes. TiO₂-nanocomposite membranes had a higher permeation drag compared to polysulfone membranes, indicating a decreased affinity to interact with HA compared to polysulfone membranes.

It was concluded that for nanocomposite membranes the nanofiller determines the chemical and physical interaction of natural organic matter with the membrane surface. Both ZnO and TiO₂-nanocomposite membranes showed an enhanced pure water permeation, ZnO nanocomposite membranes had a higher permeation rate, which translated to a higher permeation drag ultimately increasing fouling. The chemical interaction of nanoparticles and foulants was caused by the release of cations from nanoparticles surface or due to chemical interaction between foulants and nanoparticles surface.

Chapter 1: Introduction

Water is essential to life. Unfortunately, 1 billion people around the world lack access to clean water and 2.7 billion people are living in water stressed countries (1). In other words, almost 40% of the world's population are suffering due to lack of access to clean water. Jordan is one of the most water stressed countries in the world, with a current 200 cubic meter per person (2). It is projected that Jordan water shortage will become increasingly severe, and by 2025 water supply will fall by half (2,3).

Membrane based operations may provide a solution to the water shortage problem. By providing cleaner water at industrial scale. Ultrafiltration membranes may be used to reclaim polluted water resources from pathogens, colors and organic molecules (4–6). However, membranes suffer from a decline in performance with time. This decline is due to the accumulation and/or precipitation of suspended and/or dissolved matter (foulants) found in the feed water (4,5). This adds to the operational costs of membrane-based water treatment operations.

Recently, nanotechnology and nano-sized materials have been studied extensively for their unique properties and endless applications. If nano-sized materials are incorporated in the membranes structure, then an enhancement in membrane properties is expected. Reducing membranes interaction with foulants and enhancing water permeation are the main goals of fabrication of nanocomposite membranes.

Despite their many advantages, polysulfone (PS) ultrafiltration membranes performance is hampered by fouling. Fouling causes a decline membranes flux and adds to the operational costs of membrane-based water treatment operations. It is proposed to mitigate fouling by adding hydrophilic material in the casting solution or in the gelation bath.

Nano-sized metal oxides have been chosen as modifying agents and added to the polysulfone solution. Nano-sized metal oxides have been chosen due to their hydrophilic nature. Zinc oxide (ZnO) and titanium dioxide (TiO₂) were chosen because of their commercial availability, stability and lack of studies conducted on ZnO and TiO₂ nanocomposite membranes fouling with humic acid, especially at NP's concentrations exceeding 1wt% in the casting solution. Nanocomposite membranes interaction with humic acid is expected to be different than PS membranes. Due to expected changes in internal structure, surface morphology, surface hydrophilicity and membrane composition i.e. chemical composition.

A literature review of membranes and membranes fabrication techniques is provided in chapter 2. Chapter 2 provides a more detailed analysis of membranes fouling and membranes modification. A literature survey regarding the fabrication of nano-composite membranes specifically ZnO and TiO₂ nanocomposite membranes is also provided in chapter 2. The experimental procedure used to fabricate ZnO and TiO₂ nanocomposite membranes is provided in chapter 3. The techniques used to characterize membranes and further analyze them is also provided in chapter 3.

The results and discussion of ZnO nanocomposite membranes are presented in chapter 4. The chapter starts with discussing the pure water permeation of ZnO nanocomposite membranes. Followed by a study of membrane surface morphology and internal structure. Performance of ZnO nanocomposite membranes during fouling experiments and their

interaction with humic acid is outlined and discussed. Finally conclusions are drawn regarding ZnO nanocomposite membranes, performance and interaction with humic acid.

Chapter 5 is dedicated to discussing results of TiO₂ nanocomposite membrane performance and structure are presented and discussed. The pure water permeation of TiO₂ nanocomposite membrane is discussed. Surface morphology and internal structure of TiO₂ nanocomposite membrane is presented and discussed. Performance of TiO₂ nanocomposite membranes during fouling experiments and their interaction with humic acid is outlined and discussed. Finally conclusions are drawn regarding TiO₂ nanocomposite membranes, performance and interaction with humic acid.

Chapter 2: Literature Review

2.1 Membranes

Membranes have become an integral part of water treatment applications (4–6). These applications extend from water purification—pathogens, colors, organic molecules etc.—to water desalination (4–6). Membranes function by allowing certain (acceptable or desired) molecules to pass through it while preventing or rejecting other (undesirable) molecules to pass. A simple idealized representation of the separation of solute and solvent using membranes is shown in Figure 1. While the function of membrane is easily understood, the actual mechanisms involved in separation can be quite involved.

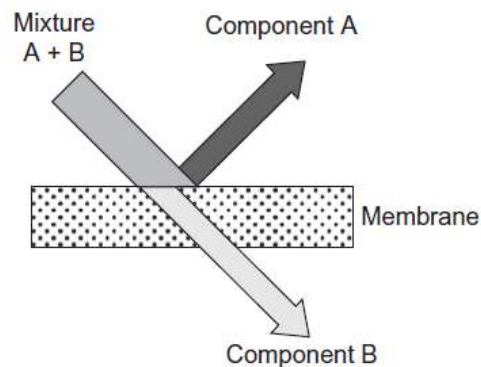


Figure 1: Schematic sketch of membrane separation (7).

Currently, pressure driven membranes, in which the driving force for separation is provided by mechanical pressure, are the industrial standard for membrane processes (6). Pressure driven membranes include as ultrafiltration (UF), nanofiltration (NF) and reverse osmosis (RO) (4).

RO membranes are used in water desalination and purification (1). The diameter of RO membrane pore ranges between 0.2 nm-0.5 nm, which allows water to pass through the membrane and retains ions and cations (3). The flux through RO membranes is described

using solution- diffusion model (1).

UF membranes on the other hand are porous, with pores ranging from 1nm to 200 nm in diameter (6). The flux through UF membranes is due to the laminar flow of fluid inside the pores of the membrane, which is described using Hagen-Poiseuille law (8). NF membranes are considered an “intermediate” membrane between RO (non-porous) and UF (porous) membranes (4). NF membranes pores range from 0.5 nm to 1 nm in diameter, which means that flux is due to solution-diffusion and to flow through pores (4). RO,NF and UF membranes are capable of achieving good separation and flux at relatively low cost (8). Figure 2 shows the separation performance of the different types of membranes.

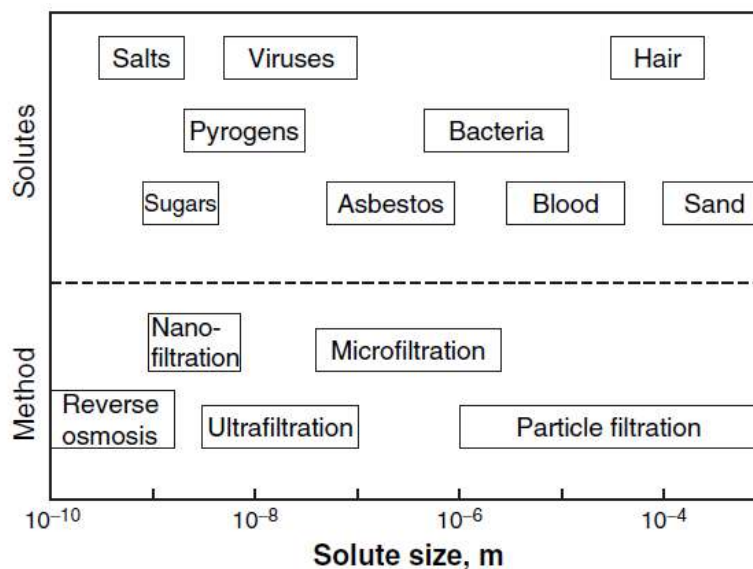


Figure 2: Membranes Used to Achieve Good Separation of Different Solutes. i.e. RO is Used to Remove Salts, While UF is Used to Remove Viruses (8).

Owing to the fact that the separation capabilities of membranes are highly dependent on their morphology, membranes are characterized by their internal structure (4,8). Membranes can be classified as symmetric and asymmetric based on their internal structure (4,5,8,9). Each of these types be further classified into subclasses based on the

nature and materials used in their synthesis. Figure 3 shows a schematic sketch of different membrane structure.

Symmetrical membranes have no variations in their cross sectional structure and the flux and rejection are determined by the entire structure (4,8,9). The drawbacks of symmetrical membranes are their low flux due to their thickness (4,8). Thus, these membranes are less important commercially, but considered useful in laboratory studies (4,8)..

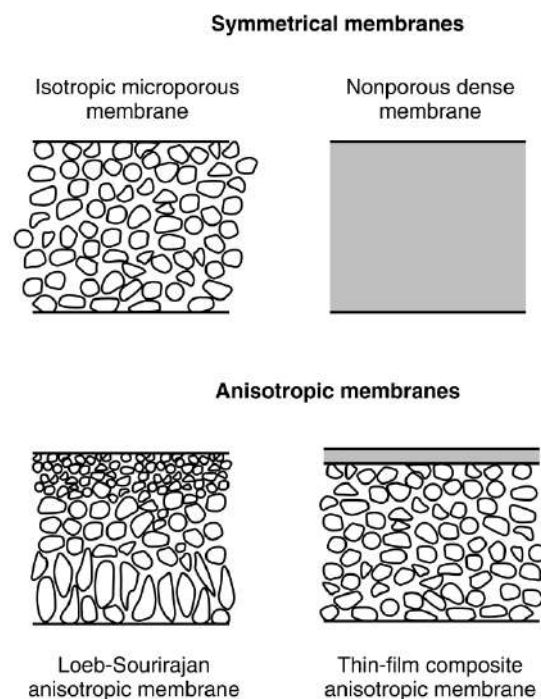


Figure 3. A schematic sketch of symmetrical and asymmetrical membranes (4).

Asymmetrical membranes provide better flux and selectivity compared to symmetrical membranes (4,6,8). The structure in these membranes varies in porosity from a very dense layer at the top to larger pores at the bottom (4,8-9). Figure 4 shows an SEM cross-sectional image of porous asymmetric UF membrane.

The dense layer (also called selective or active layer) is very thin and could be porous or nonporous. It could also be made from the same or different material as the rest of the membrane (8-9). This unique structure allows the membrane flux and selectivity to be

controlled by a thin dense layer, while the rest of the membrane acts as a support to the dense layer (4,8-9).

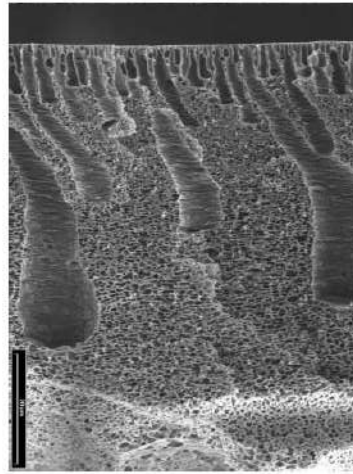


Figure 4 SEM cross section of asymmetric Poly(vinylidene fluoride) membrane. The top layer (active layer) has finger-like structure and the sub-layer has a sponge like structure (5).

The techniques used to fabricate an asymmetric membrane varies according to the required membrane structure and separation (4,6,8,10). Phase inversion is used to create UF membranes with asymmetric internal structure (4,6,8,10). Interfacial polymerization is used to create NF and RO membranes (4,6,8). Solution casting is used to create membranes with thin active layer by physical means rather than chemical means (4,6,8,10). The techniques used to fabricate membranes are further elaborated in the following section.

2.2 Membrane Fabrication

Membrane structure determines its flux and rejection and, ultimately, the process for which the membrane is suitable (4,8-9). The internal structure of the membrane is determined during the fabrication step. This section will elaborate the three techniques used to fabricate asymmetric membranes: phase inversion, interfacial polymerization and solution casting.

2.2.1 Phase Inversion

The first asymmetrical membrane, called the Loeb-Sourirajan membrane, was fabricated using phase inversion method (11) and resulted in better flux and rejection than symmetrical membranes (4,11). The phase inversion process depends on the idea of separating a homogenous cast solution into two separate phases (4,6,9).

There are four methods to obtain membrane using phase inversion (4,10). The first is thermally-induced phase inversion, where the cast solution is heated and allowed to cool, the change in temperature causes formation of the porous membrane structure. Solvent evaporation is another method where a cast solution composed of several solvents, one of which is more volatile than others, is allowed to evaporate. The highly volatile solvent evaporates at a faster rate than the other solvents causing a change in the solution composition resulting in demixing and formation of the membrane (4,10). A third method is water vapor absorption where the solution is cast on a glass plate and placed in a humid environment. Water vapor is absorbed by the cast solution inducing demixing. The most commonly used method to prepare asymmetrical UF membranes is referred to as the Loeb-Sourirajan technique or immersion-precipitation (4,11–17).

Fabrication of membranes by immersion precipitation is a simple one-step procedure. In this process, a polymer solution is made using water-soluble solvent. The solution is cast on a proper substrate (e.g. glass plate or non-woven polymeric structure) and then immersed in a non-solvent (usually water) (4,6,9). A list of most commonly used polymers are presented in Table 1. A membrane is formed due to the flux of solvent from solvent rich casting solution to solvent poor coagulation bath (Figure 5), and the precipitation of the polymer on the substrate (4,6,9). Casting solution is a term used to refer to the polymer solution (polymer and solvent) as well as any other additives to the solution.

Table 1 The most commonly used polymers in phase inversion (immersion precipitation), their advantages and disadvantages

Type Of Polymer	Advantages	Disadvantages	Ref.
Cellulose Acetate (CA)	Hydrophilic Low cost Flexible	Low Thermal resistance (<30°C) Low chlorine resistance low biological resistance	(4),(10)
Polysulfone (PS)	High mechanical strength Wide pH tolerance (1-13) High thermal resistance Flexibility in membrane fabrication	Hydrophobic nature	(10)
Polyethersulfone (PES)	High mechanical strength Wide pH tolerance (1-13) High thermal resistance Flexibility in membrane fabrication	Hydrophobic nature	(18)
Poly(vinylidene fluoride) (PVDF)	High thermal stability High mechanical stability	Hydrophobic	(19)
Polyamide (PA)	High mechanical strength Wide pH tolerance (1-13) High thermal resistance	Poor chlorine resistance	(4,10)

Interaction between solvent and polymer used has been found to affect final membranes properties i.e. morphology and porosity. Non-porous membrane is fabricated when the miscibility between solvent and polymer is low (20). In other words, increasing the miscibility of polymer in solvent increases membrane porosity (20). The most widely used types of solvents are aprotic and polar in nature (20). Aprotic solvent don't have hydrogen atoms that can contribute to the formation of hydrogen bonds (20). The lack of hydrogen bonds between non-solvent (usually water) and aprotic solvent causes rapid precipitation during immersion precipitation (20). Some of the most widely used solvents are N-methyl-2-pyrrolidone, dimethyl formamide, dimethyl acetamide or dimethyl sulfoxide (4).

Membranes structure and porosity is determined by the rate of exchange of solvent (J_{solvent}) and non-solvent (J_{water}) during immersion precipitation (5). MF membranes is formed when J_{solvent} is almost equal to J_{water} (20). On the other hand, UF membranes are formed if J_{solvent} exceeds that of J_{water} (20). There are two distinct features of UF membranes structure, finger like or sponge like membranes (5).

Finger-like membranes have been found to contain “macrovoids” in the sublayer (5). Macrovoids are elongated cavities found beneath the active layer of the membrane. Macrovoids contribute to the mechanical instability of a membrane because of their tendency to collapse under pressure (5). Macrovoids formation can be suppressed by changing the rate of solvent and non-solvent exchange during phase inversion process (5).

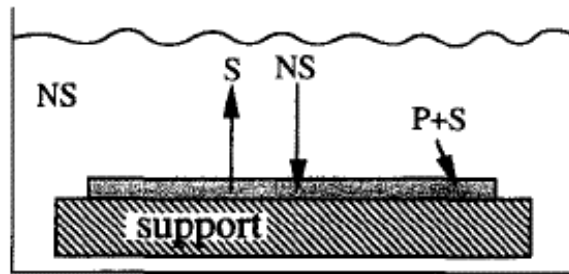


Figure 5. Schematic depiction of the immersion precipitation process (21).

The rate of exchange of solvent and non-solvent is a function of several parameters (5). These parameters include: the choice of solvents, choice of additives, viscosity of the casting solution, temperature of the coagulation bath, and temperature of the cast solution (19)–(23). If the process is a combined dry and wet phase inversion, the time of dry phase inversion prior to the immersion precipitation also affects the rate of exchange between solvent and non-solvent. By controlling these parameters a membrane with specific morphology can be obtained.

Phase inversion process on a ternary phase diagram is illustrated in Figure 6 (25). Point A represents the initial cast solution state prior to casting. During casting the polymer-

solvent composition changes and reaches the boundary line B. At this point two phases are formed, a polymer-rich phase shown in the upper boundary line and polymer-poor phase shown in the lower boundary line. The point of membrane precipitation occurs when the casting solution composition changes and crosses the tie line connecting the poor-polymer phase and rich-polymer phase D. At this point the structure of the membrane is determined. Point C is the final membrane and it is a mixture of a solid polymer membrane (point S) and liquid non-solvent (point L) (25).

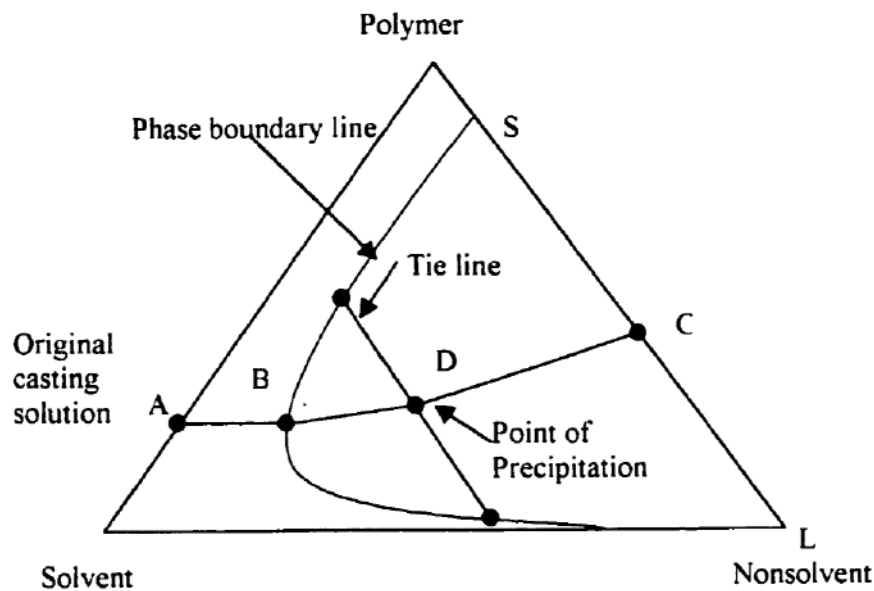


Figure 6. The ternary phase inversion system and the membrane formation mechanism (25).

Inspection of Figure 6 shows that membrane precipitation can occur at any point on the tie line (not only D), hence membrane structure is also determined by the point in which the tie line is crossed (5). In other words, the membrane formation mechanism is determined by the path between points B and D (5,25). The two mechanisms by which polymer films are formed are spinodal decomposition (SD) and nucleation growth (NG) (5). SD forms membranes with interconnected pore structure, while NG forms closed pores that continue

to grow and might be interconnected if given enough time (5). Both SD and NG are determined by the speed of demixing i.e. the speed solvent and nonsolvent diffusion (6).

Polymer precipitation and membrane porosity are affected by the gelation bath temperature (23,25,27). As temperature increases, the rate of solvent non-solvent exchange increases, larger pores and less porous membrane is fabricated (4,10,27). The rate of solvent and non-solvent exchange is affected by temperature because diffusivity is a function of temperature (8).

Changes in gelation bath conditions are reflected on the ternary phase diagram (Figure 6). By changing the point at which the tie line is crossed, membranes with desired morphology (pore size and porosity) can be obtained. Figure 7 shows the different pathways of membrane formation on a phase diagram (28).

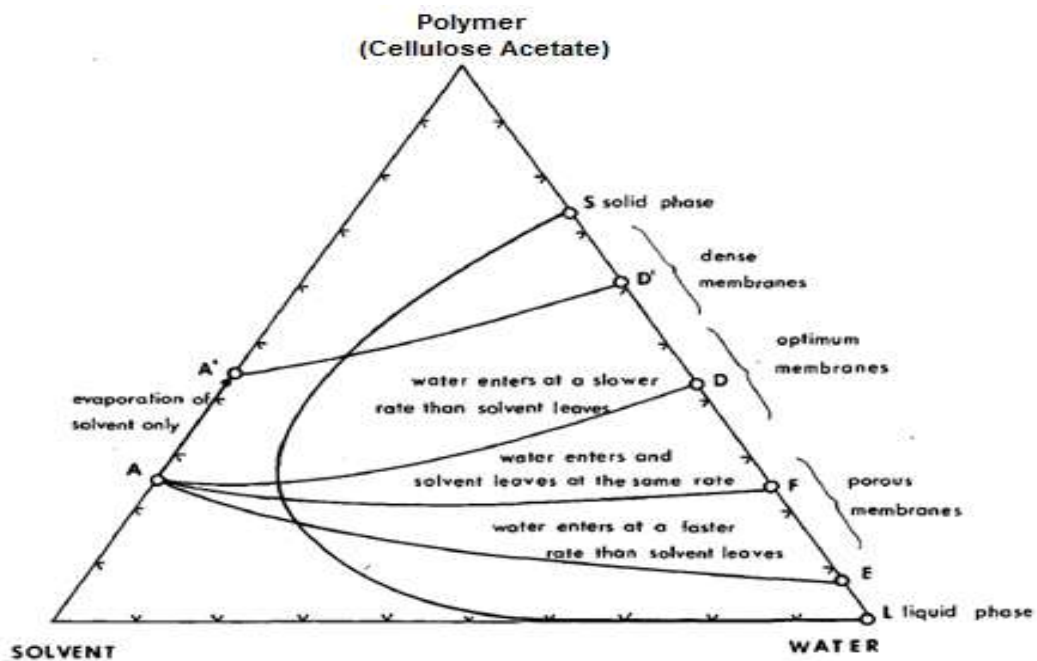


Figure 7 The membrane formation pathways based on different solvent non-solvent exchange rates and the final membrane structure obtained following each pathway (28).

For example macrovoids formation can be suppressed if the polymer concentration in the casting solution is increased, hence increasing solution viscosity. Another way to manipulate the viscosity of the casting solution is by adding a cross-linking agent to the polymer solution. Changing the solvent or adding a solvent to the gelation bath are also ways in which macrovoids formation is suppressed by changing the rate of solvent/non-solvent exchange (5).

2.2.2 Interfacial Polymerization

Interfacial polymerization (IP) is used to create composite membranes with a very thin selective layer (in the submicron scale) on top of a porous support layer (typically made by phase inversion) (4,6,8, 10-29). Membranes fabricated by interfacial polymerization are called thin film composite (TFC) membranes and are used in NF and RO applications (4,6,8, 10-29).

In the IP process, an aqueous solution of a reactive monomer is pressed onto the top layer of a porous support membrane (10,30,31). The most commonly used monomer is m-phenylenediamine (MPD), but other monomers such as piperazine, N-N'-diaminopiperazine, N-(2-aminoethyl)-piperazine are also used. The monomer loaded membrane is then immersed in a water immiscible solution containing another reactive component (usually trimesoyl chloride, TMC) (4,5,8,10,30). The aqueous and organic phases form two layers and the polymerization reaction will take place at the interface and propagates to create a highly cross-linked layer on top of the support layer (4,8,10,30). This newly formed layer is referred to as the active layer, and it controls the flux and rejection of membrane (4,6). The porous structure beneath it serves as a mechanical support for the active layer (4,6,8). The structure of a TFC membrane is shown in Figure 8.

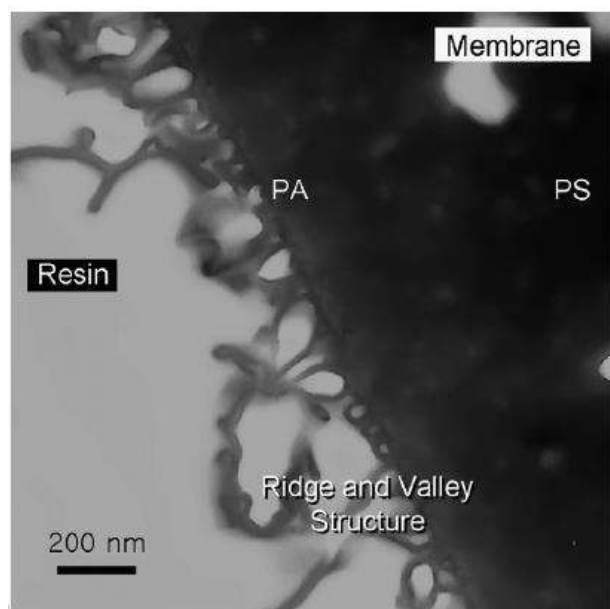


Figure 8 TEM images of TFC of commercial RO membrane (ESPA3). The structure of the thin polyamide (PA) layer is highly non-uniform. The polysulfone sublayer shows the presence of large pores (32).

RO and NF performance is affected by the choice of monomer used to fabricate the active layer (10,30,33). Polyamides exhibit high biological and chemical resistance, have high flexibility and have long service life. Therefore, polyamide membranes fabricated from aliphatic/aromatic diamine are the most successful TFC membranes on a commercial scale (30,33). Despite the commercial success of polyamide membranes, research on the advancement of commercial RO and NF, improved flux and longer lifetime, is ongoing field of research (30,34–38).

2.2.3 Solution Coating

Solution coating is somewhat similar to interfacial polymerization method; both methods create thin film composites with highly dense active layer (4,9). However, solution coating method depends on physically attaching the active layer to the membrane surface (4,9). The coating is done using a dilute polymer solution, where the solvent is volatile and immiscible in water (4,9). The solution is cast on the surface of water and a thin film is formed (4,9). A micro porous membrane is then covered by the film and dried (4,9,20).

This procedure is very simple but defect free membrane is hard to obtain, especially when the desired active layer thickness is less than 1 μm (4,9).

Finally, one can gather that membrane performance is determined during fabrication. Therefore, different processes require different membranes e.g. RO for desalination and UF for water purification. Thanks to different fabrication techniques, membranes with high performance and low energy consumption are obtained, making membranes a commercial success (4,39). However, membrane based processes suffer from higher operational costs, because membranes performance deteriorates with time (4,39). The deterioration in membrane performance (flux) is attributed to fouling, discussed in the following section.

2.2 Membrane Fouling

Fouling is a major obstacle in membrane technology, because it reduces membrane lifetime and efficiency (4,5). Fouling may be defined as the gradual decay of membrane performance (Figure 9) due to the deposition (accumulation and/or precipitation) of suspended and/or dissolved matter (foulants) found in the feed water (4,5).

Fouling is a complicated process due to the numerous foulants and the different mechanisms by which fouling occur. Foulants are subdivided into suspended collides, microorganisms and natural organic matter (4),(40). These foulants degrade membrane performance through several mechanisms: pore blocking, biofouling and organic fouling (41,42). These mechanisms often occur simultaneously, which complicates their understanding adequately (43,44).

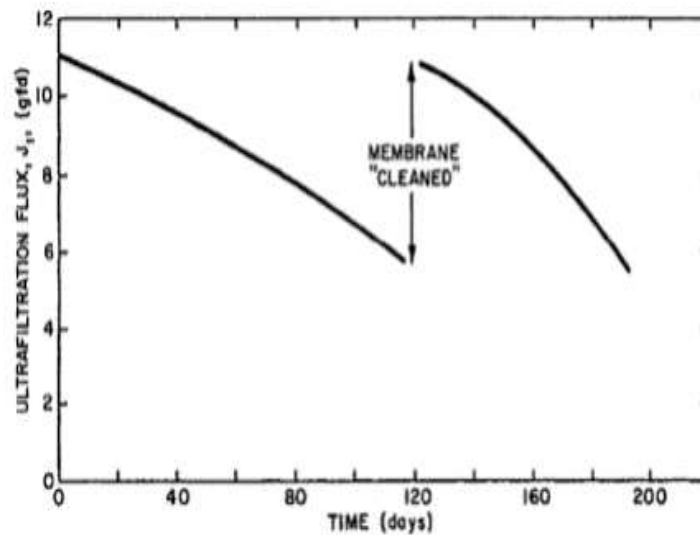


Figure 9. Flux decay due to membrane fouling and restoration of flux by cleaning (4).

Colloidal particles cause pore blocking. Example of foulants causing pore blocking are fine particular matter, algae and iron corrosion products are some (4,45). The suspended colloids are defined as “silt” and can block off membranes by four different mechanisms as depicted in Figure 10. Complete blocking is the complete plugging of pores by colloidal matter. In this type, foulants plug membrane pores without overlapping (46). Pore constriction (also called scaling) is caused by precipitation of foulants (scalants such as silica) inside the membrane pores (4,46). Pore restriction does not block the pore entirely but it reduces the free volume available for water to move, hence causes flux decline (46). Cake filtration happens in non-porous membranes (there are no pores to block) or when the pores are already blocked and foulants deposit on top of each other (46). Intermediate fouling is an intermediate mechanism between cake filtration and pore blocking mechanism (46). All four mechanisms are caused by inorganic matter such as silica.

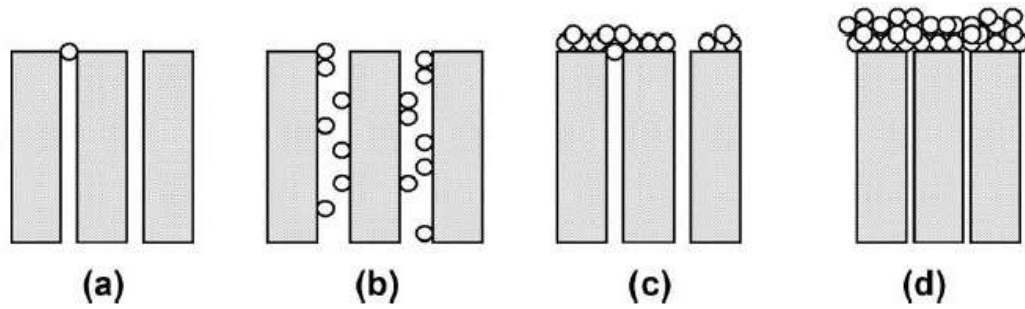


Figure 10. Different blocking mechanisms of colloidal particles: a) pore blocking, b) pore restriction (scaling), c) intermediate fouling, and d) cake filtration (46).

Bio fouling is defined as the attachment of bacterial cells on the membrane surface (4,47). Bio-fouling is a challenging problem because bacteria is able to adapt and thrive even under hard conditions (47,48). Furthermore, certain membranes such as cellulose acetate are considered a good nutrient source for bacteria (4). Biofilm formation on membrane surface (presence of bacteria and metabolic substances) has an effect on membrane performance similar to cake filtration (47,48).

Organic fouling is caused by natural organic matter (NOM) (49). NOM is composed of different biopolymers with either a hydrophobic (e.g. humic substances) or hydrophilic (e.g. polysaccharides) nature (15,50,51). Not only does hydrophobic biopolymers make up the largest fraction of NOM, they also cause the most damage (fouling) to membranes (15,50,51). The interaction between humic substances and membrane surfaces and the subsequent fouling is a function of physical and chemical parameters (40,52–55).

The chemical composition of the solution such as: pH, presence of divalent and monovalent ions and the type of foulant (molecular weight, charge etc.) are parameters affecting the fouling rate (54–56). Physical parameters effecting the membrane fouling rate include applied pressure, permeate flux, membrane surface roughness and concentration polarization (37,50,57). These parameters are summarized in Table 2.

Table 2. The Parameters Effecting Rate of Fouling by NOM.

Parameter Effecting Fouling	Rate of Fouling	Cause	Ref.
Increase in divalent ion concentration in the feed solution	Increase	Reduction in electrostatic repulsion between membrane and NOM	(54)
Increase in monovalent ions in the feed solution	Increase	Reduction in electrostatic repulsion between membrane and NOM	(54)
Increase in pH of solution	Decrease	Reduction in electrostatic attraction between membrane and NOM	(54)
Increase in the hydrophobic fraction of NOM	Increase	Hydrophobic interaction	(56)
Higher Applied Pressure	Increase	Pressure might approach the “limiting flux”, where a stable membrane flux cannot be sustained	(40)
Concentration Polarization	Increase	The concentration of NOM on membrane surface higher than bulk	(57)
Permeate Flux	Increase	Permeation drag and electrostatic attraction occurring simultaneously	(58)
Rough Membrane Surface	Increase	Valley Blocking	(59)

Fouling, especially organic, is the main drawback of membrane technology. The reduction of fouling tendency has been and continue to be the motivation for many research projects focusing on improving the membrane itself. Extensive reviews are found on the subject such as Khulbe et al review and Kang et al review (60,61). The following section discusses the methods used to modify UF membranes.

2.3 Membrane Modification

It is clear from the previous discussion that fouling is a major drawback facing the membrane technology. Therefore, overcoming fouling by improving the membrane properties is the goal of many researchers by modifying the membrane surface to obtain better flux, rejection and lower fouling (39).

Membrane modification is based on changing the membrane surface properties (e.g., hydrophobicity and charge) to obtain better performance and to elongate the membrane lifetime (36,61,62). Membrane modification can be categorized into two groups: *in-situ* and *ex-situ* modifications (18). In-situ modification is the modification of the polymer bulk material (casting solution) prior to or during membrane fabrication. Ex-situ modification is the modification of an already fabricated membrane; it usually refers to surface modification of membranes by different means.

Ex-situ modification is used to increase flux, improve salt rejection and reduce fouling by changing or modifying the membrane surface (18,61). Several methods have been used to achieve these goals including: radical polymerization (35,63), photochemical techniques (36), low temperature plasma (13), layer-by-layer alternating polyelectrolyte deposition (APD) (64) and ionizing radiation (65). Unlike in-situ techniques, ex-situ modifications enhance the membrane surface characteristics, but do not change the membrane inner structure.

In-situ modification is concerned with improving membrane inherent characteristics such as: the chemical composition of the membrane, morphology and structure (10,18,61). The morphology and structure are important parameters in determining a membrane flux and rejection (10,18,61). The chemical composition of the membrane can determine the membrane affinity towards foulants (10,18,61).

In-situ modification may be achieved by changing membrane bulk material prior to fabrication. This change can be induced by chemical reactions such a sulfonation and carboxylation of the bulk polymer (66,67), or blending the bulk polymer with different materials (14,68,69). Another route to achieve *in-situ* membrane modification is by modifying the membrane during fabrication by changing fabrication conditions (70).

2.3.1 Blending Method

Blending method is a simple modification technique, which involves addition of additives to the cast solution. Additives can be used to obtain a certain morphology e.g. suppress macrovoids formation. Additives have been found to enhance hydrophilicity and enhancing flux (12,13,68). Polymers, monomers, inorganic materials and nanoparticles are some of the additives used in the casting solution. This section aims to explore the blending method more thoroughly.

Lee et al (12) studied the effect of adding different concentrations of PVP to the cast solution of PS membranes prepared by phase inversion. It was found that addition of PVP enhances demixing during phase inversion. It was found that a PVP concentration below 10 wt% causes macro voids formation, i.e. finger like structure as shown in Figure 11, whereas a concentration higher than 10 wt% suppressed macro voids formation. This was attributed to the rheological hindrance effect, i.e. kinetic hindrance. The water permeability was found to exhibit a maximum at a PVP concentration of 7.5 wt%. Further addition of PVP did not enhance the flux even though the rate of phase inversion was enhanced.

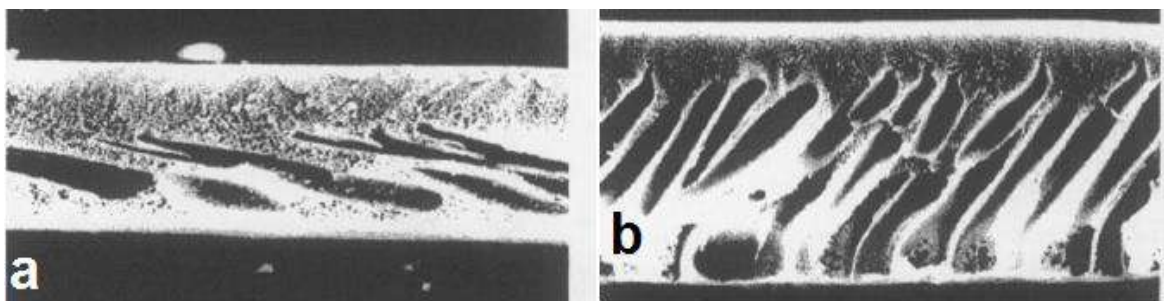


Figure 11. SEM images of PS membranes prepared with: a) no PVP, and b) 7.5 wt% PVP in the cast solution (12).

Zhao et al (17) conducted a study where they used a novel additive composed of polyaniline-polyvinyl pyrrolidone-nano-composites (PANi-PVP) to PS membrane casting solution. Addition PANi-PVP was meant to enhance the hydrophilicity of the membrane

surface. It was found that part of the PVP leached out of the casting solution during phase inversion and acted as a pore forming agent (17). Pure water permeability of PANi-PVP/PS membranes was almost double that obtained from PVP/PS membranes, as shown in Figure 12.

The fouling recovery ratio experiments were carried on PANi-PVP/PS. Fouling recovery ratio (FRR) is defined as the ratio of pure water flux after membrane fouling to pure water flux prior to membrane fouling. Fouling recovery ratio is used to indicate anti-fouling properties of membranes. Fouling recovery ratio of PANi-PVP/PS was reported to be 76-84% compared to 70-74% obtained from PVP/PS membranes (17). The authors claimed that this result was proof of an improvement of antifouling properties of PANi-PVP/PS membranes.

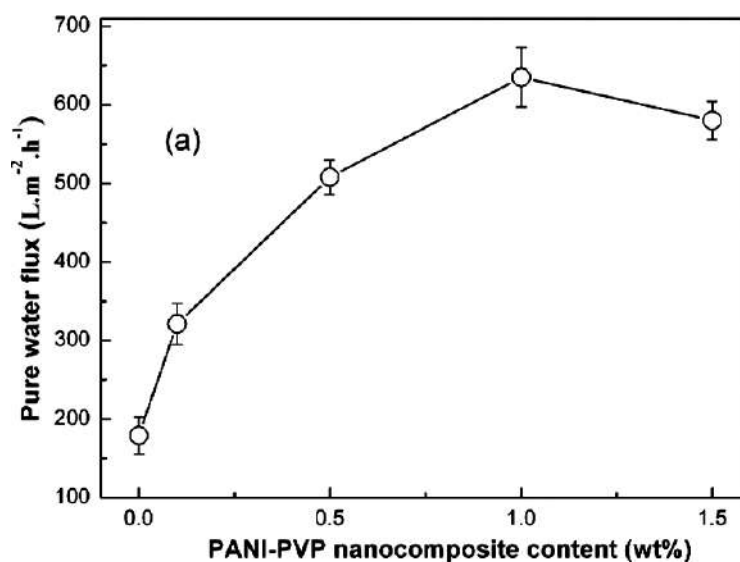


Figure 12. Pure water flux of PANi-PVP-modified PS membranes (17).

Another study using emeraldine base polyaniline (PANiEB) as a pore forming agent and a hydrophilic modifier in PS membranes was conducted by the same group (16). The choice of PANiEB was based on its solubility in the casting solution and low solubility in water; PANiEB will migrate with the solvent during phase inversion process and remain at the membrane surface due to its low solubility in water, rendering the membrane surface more

hydrophilic. Because it is slightly soluble in water it is less likely leached out during operation. Cross sectional SEM images showed macro voids formation decreased for PANiEB/PS membranes and was replaced by fingerlike interconnected structure.

PANiEB concentration in the casting solution was found to have a turnover point similar to that found by Lee et al (12) for PVP/PSF membranes (25). As can be seen in Figure 13, the turnover occurs at a PANiEB concentration of 0.1 wt% which has a maximum water permeability. Increasing the concentration beyond 0.1 wt% causes a rapid decline in water permeability. SEM images of the membrane surface showed that the porosity and pore size of the membrane increased with concentration in the region below 0.1 wt%. Beyond this point, porosity and pore size decreased. This was attributed to the high casting solution viscosity, which hindered the movement of PANiEB and consequently reduced the pore forming effects (16).

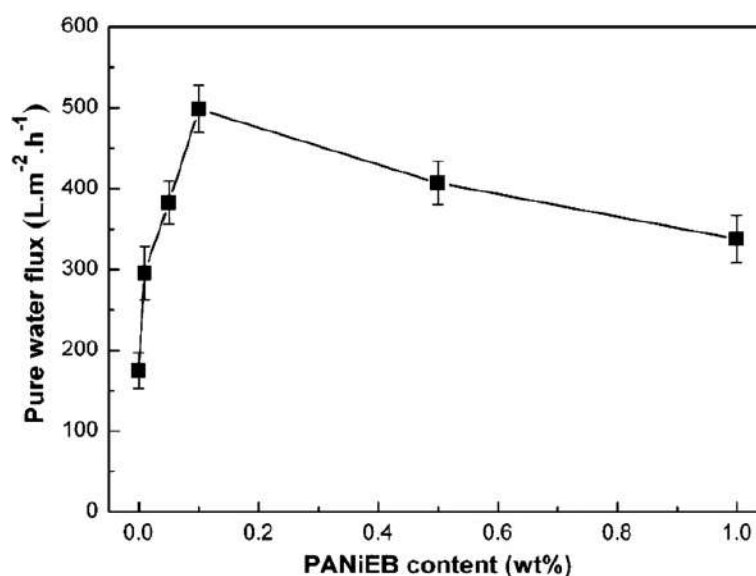


Figure 13. Pure water permeability of PS membranes containing different PANiEB concentrations (16).

From the above studies it can be concluded that addition of hydrophilic monomers and polymers to the casting solution has been found to enhance membranes hydrophilicity and flux (12,13,68), (61). In recent years, there has been an inclination to use nano-sized as

modifying agents in the casting solution and the subsequent fabrication of nanocomposite membranes. The following section details some studies in which nanocomposite membranes were fabricated.

2.3.2 Fabrication of nanocomposite membranes

More recently, researchers have been interested in the possibility of adding nanomaterials to the casting solution to create membranes with specific properties, e.g. biocidal membranes and membranes with high mechanical stability (14,71,72). Nanomaterials are interesting because they exhibit different properties than their bulk material counterparts (73). Another advantage of using Nanomaterials is their high surface area to volume ratio, which increases their reactivity (73). But the most interesting advantage is the ability to tune Nanomaterials based on their size and the ability to be further functionalized by different means (73).

Despite their many advantages, nanoparticle tends to aggregate easily during processing, which reduces their efficiency (74). Aggregates are formed due to the high surface area of nanoparticles (NP's) compared to their bulk counterparts (75). Reduction of nanoparticles aggregation requires modification of nanoparticles surfaces. Modification of nanoparticles surface is achieved physical means or chemical means. such as coating or such as monomer or polymer grafting on nanoparticles changes the original properties of nanoparticles (72,74,76). Nanoparticle modification might be advantageous in membrane technology, because aggregates might block membranes pores during filtration thus causing a decline in flux. However, changing the properties of nanoparticles due to surface modification changes foulant nanocomposite membrane interaction.

Nair et al (14) used polyether glycol (PEG) as a pore forming agent and calcium carbonate nanoparticles (CCNP's) as a hydrophilic modifying agent to enhance PS membrane

performance and antifouling properties. Water permeability of the resulting composite membrane increased with increasing CCNP concentration. The authors attributed this to the decrease in the thermodynamic stability of the cast solution as the concentration of CCNP and PEG increased. They claimed that the decrease in thermodynamic stability changed the membrane morphology, i.e. increased membrane porosity, as seen in cross sectional SEM images of the membranes (Figure 14). An increase in porosity in the sub-layers of the membranes as CCNP concentration increased is clearly seen.

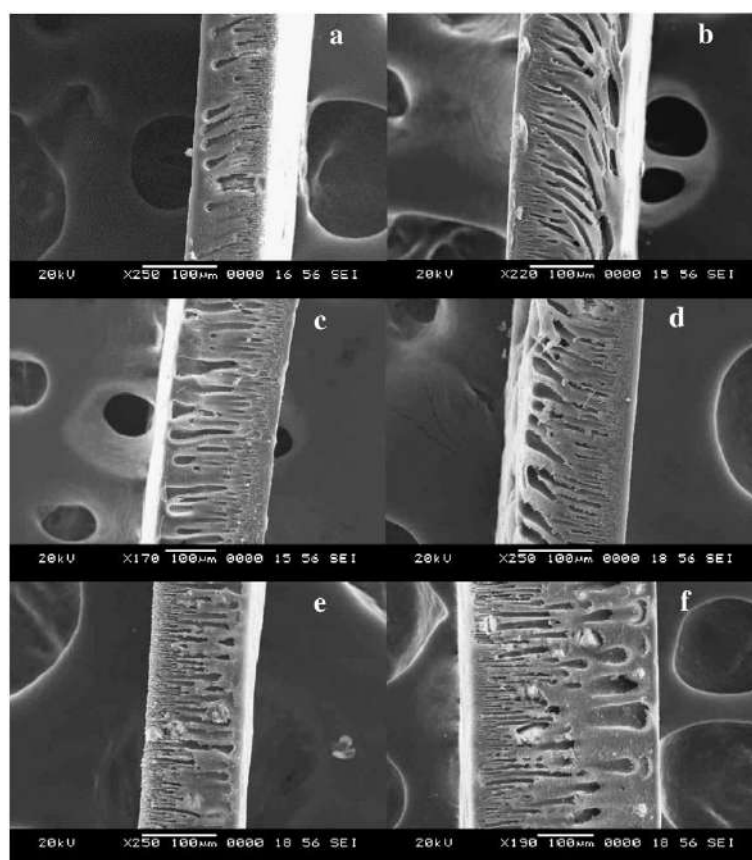


Figure 14. SEM images of cross sections of PS membranes modified with PEG and CCNP: a) 0:0, b) 0:5, c) 1:5, d) 2:5, e) 5:5, and f) 10 CCNP:5 PEG (wt%) (14).

The membrane performance was tested using BSA solution, and the flux decline for all membranes was similar (14). The fouling recovery ratio increased with increasing CCNP concentration. There was no turnover point reported in Nair et al (14) work even though CCNP concentration in the casting solution was as high as 10% (14). This was attributed

to the fact that changes in solution viscosity was not very high. Therefore, CCNP dispersion was not inhibited.

Another study conducted by Crock et al (26) used exfoliated graphite nano-platelets (xGnP) “decorated” by gold nanoparticles (AuNP’s) as nanofillers in PS membranes (26). High water permeability of PS membranes (in the range of 20-120 L/m².hr.bar) were reported. They also reported high variations in the data recorded for the modified membranes. Figure 15 shows the compaction behavior of several bare xGNPs-AuNP-loaded PS membranes. The PS membranes modified with xGNPs-AuNP exhibited higher water permeability, lower flux decline rates and lower variations than that of bare PS (26).

Compaction of xGNPs-AuNP/PS membranes was lower compared to PS membranes. This was attributed to an increased mechanical strength of xGNPs-AuNP/PS membranes, which prevented membrane deformation by pressure (26). Figure 15 shows the permeability of PS and 1% xGNPs-AuNP/PS membranes with respect to time. The decline in flux is due to deformation of internal structure of membranes.

SEM images of such membranes is shown in Figure 16 shows a schematic sketch of the change in membrane morphology as a function of membrane xGNP loading (26). It is shown that as xGNP loading increases in the casting solution, membranes show an increase in macrovoids formation. Macrovoids contribute to the mechanical instability of membranes and subsequent loss of flux during initial stages of operation (compaction). However, Figure 15 showed that despite having larger macrovoids (Figure 16) 1 wt% xGNPs-AuNP/PS membranes had a lower decline in flux due to compaction. This might indicate that macrovoids formation is not the only contributing factor when it comes to pre-compaction. Crock et al attributed the lower flux decline despite macrovoids

formation to an increase in membranes porosity as a function of xGNPs loading in PS membranes.

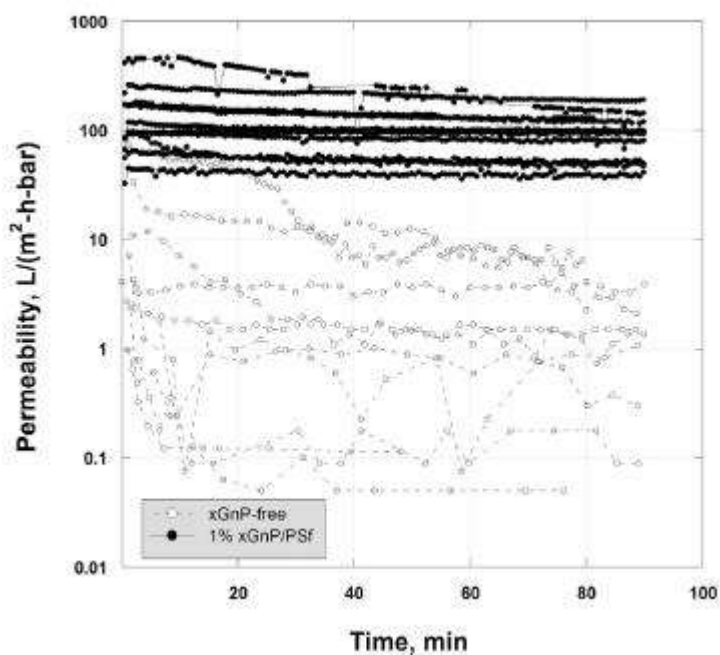


Figure 15. Compaction behavior of bare PS membranes and 1wt%xGNPs-AuNP composite membranes (26).

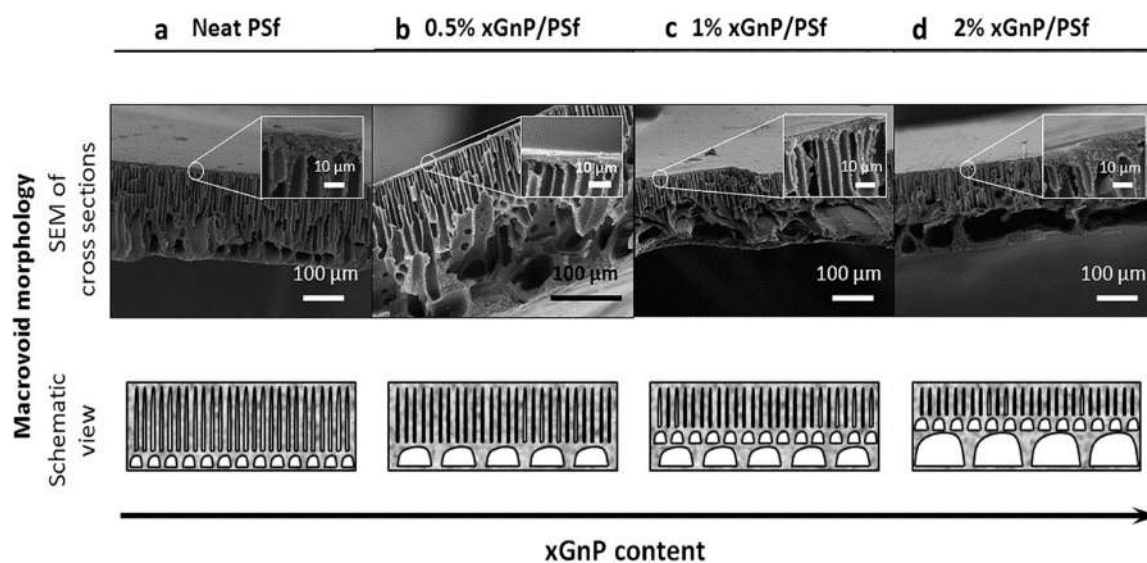


Figure 16. SEM images of cross sections of bare and composite (with xGnP) PS membranes. Also shown is a schematic sketch of the membrane macrovoids formation in the sublayer as a function of xGnP content in the cast solution (26).

The short review of nanocomposite membranes presented gives a scope to the range of nanoparticles that could be incorporated into membranes casting solution. Silver nanoparticles (47), carbon nanotubes (77), nano-clays (78), metal nanoparticles (79) and silica nanoparticles (17) are some of the recently employed nanoparticles in membrane modification via blending with casting solution. The wide range of materials used and different applications in membranes modification is the topic of some excellent review papers (80,81). However, this thesis focuses on two types of metal oxide nanoparticles interaction with humic acid. These particles are titanium dioxide (TiO_2) and zinc oxide (ZnO). A review for the incorporation of TiO_2 in the polymer matrix is presented in the following section.

2.3.2.1 Titanium Dioxide (TiO_2) Nanocomposite membranes

Yang et al (82) studied the fabrication of PS/ TiO_2 nanocomposite membranes. Where surfaces of TiO_2 NP's were modified by using sodium dodecyl sulfate. Modification was meant to enhance TiO_2 NP's dispersibility. Modified TiO_2 concentration used in the casting solution was 1, 2, 3 and 5 wt%.

PS/ TiO_2 nanocomposite membranes exhibited an increase in porosity as the modified TiO_2 concentration in the casting solution increased with increasing modified TiO_2 concentration. Water permeability of PS/ TiO_2 nanocomposite membranes reached a maximum ($488 \text{ L/m}^2\cdot\text{hr}\cdot\text{bar}$) when modified TiO_2 concentration was 2 wt% and subsequently decreased at higher concentration reaching a minimum ($250 \text{ L/m}^2\cdot\text{hr}\cdot\text{bar}$) at 5 wt% TiO_2 . The PS membranes were reported to have water permeability of $280 \text{ L/m}^2\cdot\text{hr}\cdot\text{bar}$. The initial improvement of flux was attributed to the increased porosity and improved hydrophilicity i.e. decrease in contact angle measurement as modified TiO_2

concentration increased. However, the formation of aggregates at concentrations higher than 2 wt% caused a decline in water flux.

Fouling of PS/TiO₂ nanocomposite membranes was carried out using bovine serum albumin (BSA). Fouling tests were only carried out for 2% PS/TiO₂ nanocomposite membranes. PS membranes showed a decrease in flux by $\approx 50\%$ while 2% PS/TiO₂ nanocomposite membranes showed a decrease in flux by $\approx 11\%$. Indicating an improved anti-fouling properties of PS/TiO₂ nanocomposite membranes.

Bae et al (83) used TiO₂ (0.1-0.5wt%) as an additive in PS membranes. PS/TiO₂ nanocomposite membranes showed a decrease in water flux and a decrease in rejection as TiO₂ increased. The decrease in flux and rejection was attributed to TiO₂ clogging the pores of the nanocomposite membrane during phase inversion. Thus reducing the overall porosity of membrane and at the same time keeping the larger pores open, thus reducing PS/TiO₂ nanocomposite membranes rejection.

The fabricated PS/TiO₂ nanocomposite membranes were mitigate fouling in activated sludge filtration. PS/TiO₂ nanocomposite membranes showed an enhanced flux (Figure 17) compared to that of PSF membranes. This was attributed to the increase in hydrophilicity of PS/TiO₂ nanocomposite membranes surface.

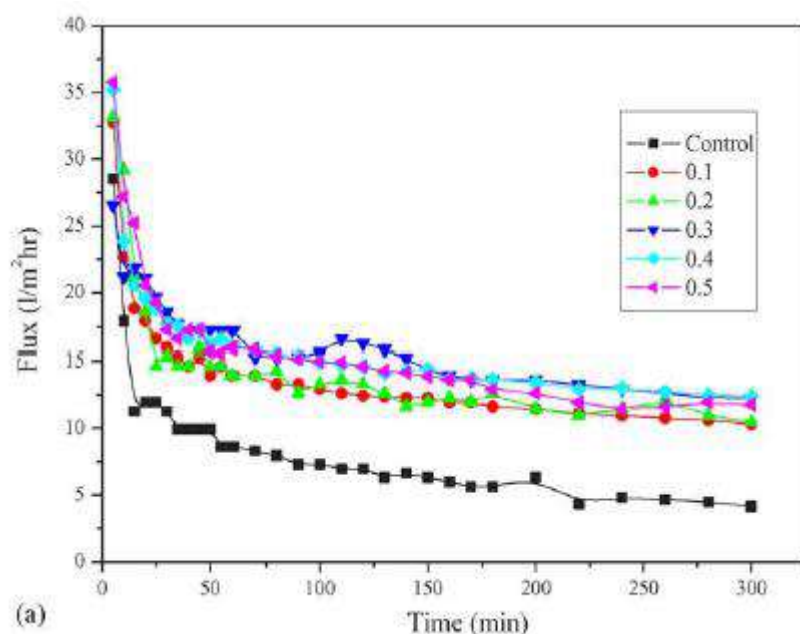


Figure 17 Flux of PS/TiO₂ nanocomposite membranes during activated sludge filtration (83)

Hamid et al (84) studied the fabrication of PSF hollow fiber membranes using PVP (5 wt%) and TiO₂ (2 wt%) as additives. Pure water permeation and porosity was found to have increased for PS/TiO₂ membrane compared to PS membrane. Fouling experiments were carried out using HA. PS/TiO₂ membranes showed an improvement in flux during HA filtration by 24% compared to PS. Furthermore, FRR for PS/TiO₂ membranes was reported to be 90% compared to 53% for PS membranes.

Zhang et al (85) modified TiO₂ nanoparticles with 2-hydroxyethyl methacrylate (HEMA) polymer chains. TiO₂/HEMA nanocomposite (0.5 wt%-3 wt%) were added to polysulfone casting solution and UF membranes were fabricated. The porosity of nanocomposite membranes found to increase as TiO₂/HEMA nanocomposite in the casting solution increased. This was attributed to an increase in casting solution hydrophilicity with the addition of TiO₂/HEMA, which promoted water diffusion into the polymer film during phase inversion. Pure water flux of TiO₂/HEMA nanocomposite reached a maximum at concentration of TiO₂/HEMA 2 wt%. Fouling experiments were carried out using BSA.

At concentration of TiO₂/HEMA 2 wt% in the casting solution, membranes exhibited the lowest flux decline of 33% compared to 50% for PS membranes. The FRR of TiO₂/HEMA 2 wt% was found to be 83% compared to 72% for PS membranes.

Teli et al (72) modified TiO₂ nanoparticles with polyaniline (PANi) creating TiO₂/PANi nanocomposite. TiO₂/PANi nanocomposite concentration used in the casting solution was 0.05, 0.1, 1.0, and 1.5 wt %. The fabricated TiO₂/PANi-PS composite membranes exhibited higher water flux than bare PS membranes. 1.0% TiO₂/PANi-PS nanocomposite membranes exhibited the highest increase in water flux which was almost twice as that of pristine PS membranes. The authors attributed the increase in water permeability to an increase in membranes surface hydrophilicity.

Anti-fouling tests were carried out using humic acid (HA) and BSA. The flux decline caused by HA was \approx 33% for PS membranes compared to \approx 20% for TiO₂/PANi-PS membranes. There is an improvement in performance noted for TiO₂/PANi-PS membranes, which could be due to increased hydrophilicity. However, Teli et al stated that a “dense compact layer” was formed on top of all membranes used in HA fouling tests. This layer was attributed to accumulation of large HA molecules on the membranes. No further insight regarding possible interaction between HA and TiO₂/PANi-PS composite membranes was given.

On the other hand, BSA fouling did not show significant improvement with composite membranes (in fact, pore plugging was suspected to occur for the 0.1 wt% composite). However, fouling recovery ratio (FRR) and BSA rejection improved as a function of TiO₂/PANi loading in PS membranes. Which indicates improved anti-fouling properties of fabricated membranes.

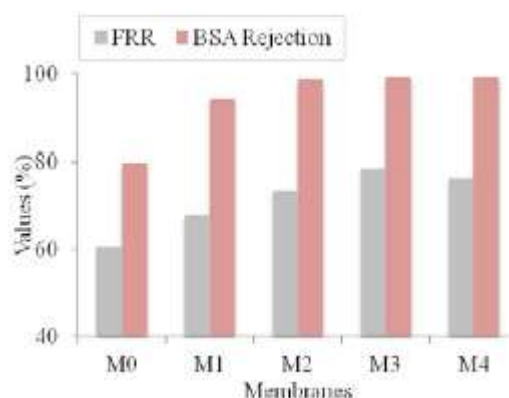


Figure 18. fouling recovery ratio and BSA rejection of PS membrane modified with different ratios of TiO₂/PANi (M0: 0, M1: 0.05, M2: 0.1, M3: 1.0, and M4: 1.5 wt%) (72).

Based on this literature survey, TiO₂ nanocomposite membranes have an improved performance even when not modified. However there is little research on the interaction of non-modified TiO₂ nanocomposite membranes with one of the most abundant foulants, namely humic acid (HA). There is a lack of a systematic study investigating TiO₂ nanocomposite membranes interaction with HA. In the following section Zinc oxide nanocomposites are looked at more closely.

2.3.2.2 Zinc Oxide (ZnO) Nanocomposite membranes

Balta et al (86) incorporated ZnO NP's into polyethersulfone (PES) membranes casting solution. Balta et al studied the change of ZnO concentration (0.035- 4 wt%) as well as the change in PES content (25-32 wt%) in the casting solution. Membranes were found to have increased pure water permeability with increasing ZnO concentration in the polymer matrix and decreased pure water permeability with increasing PES content in the casting solution. This was attributed an increase in hydrophilicity of membranes due to the presence of ZnO in the casting solution. Fouling tests were performed on 0.035, 0.125 and 0.5 wt% membranes using HA. Fouling was reduced by 25% compared to PES membranes.

Leo et al (24) fabricated nanocomposite membranes using ZnO (1-4 wt%) and (1 wt%) Polyvinyl alcohol (PVA) as additives to PS casting solution. Permeability was found to increase as a function of ZnO loading in the membrane matrix. Oleic acid was used as a model foulant and $\approx 25\%$ improvement in flux were found for 2% ZnO-PS membranes. This was attributed to the increase in hydrophilicity in membranes surface.

Hong et al (87) studied the incorporation of ZnO NP's into PVDF microfiltration membranes. ZnO (0.001-1 wt%) and PEG (3 wt%) were used as modifying agents. It was found that PVDF membranes had a rougher surface than ZnO-PVDF nanocomposite membranes when ZnO loading was below 0.005 wt%. At higher ZnO concentration an increase in membrane roughness was noted. The change in membrane roughness was attributed to filling the pores when ZnO concentration was lower than 0.005 wt%. At higher concentration, ZnO is thought to have accumulated on the membranes surface creating a rougher topography.

Hong et al (87) found that at ZnO concentration of 0.005 wt% a maximum water permeation was recorded and was twice as high as that of PVDF. This was attributed to the increase in 0.005 wt% ZnO/PVDF nanocomposite membranes pore size and porosity as well as the improved surface hydrophilicity. At higher concentrations, ZnO-PVDF casting solution was highly viscous and as a result membranes with smaller pore sizes were fabricated.

In their study, ZnO-PVDF nanocomposite membranes were tested for their anti-fouling properties using BSA. Membranes flux during fouling was not reported but FRR was reported to be the highest for 0.01 wt% membranes. 0.01 wt% membranes had the highest reported hydrophilicity of all membranes tested. This led the authors to conclude that membranes with higher hydrophilicity will have higher FRR.

Fewer studies have been published on ZnO nanocomposite membranes due to environmental safety considerations especially in aquatic environments. In a study conducted by Franklin et al it was reported that both bulk and nanoparticles ZnO have similar toxicity in fresh water because ZnO nanoparticles tend to aggregate and form larger flocs (88). Both bulk and nanoparticle toxicity is due to the release of Zn^{+2} ions in water (88). For ZnO nanoparticles, the lethal concentration (LC_{50}) for mammalian cells is reported to be 43 mg/L (in vitro study) (89). In aquatic environment, algae is found to be the most sensitive to the presence of ZnO nanoparticles ($\text{LC}_{50} < 0.1$ mg/L), followed by fish ($\text{LC}_{50} < 10$ mg/L) (89). Despite the environmental concerns of using ZnO NP's in membrane matrix modification, researchers have estimated that such concerns are diminished considering ZnO is entrapped in a solid matrix and it is not freely released to the environment (24,86,87). Furthermore, the required LC_{50} to do harm to the environment is quite high considering the low amount present (or supposedly released to the environment).

From this review, it can be concluded that the addition of ZnO nanoparticles to the cast solution affects the membrane morphology and membrane performance. Despite imparting an improved performance i.e. improved pure water permeation, at when ZnO NP's are incorporated in the casting solution at concentrations exceeding 1 wt%. There is lack on studies concerning ZnO interaction with humic acid especially at higher concentrations i.e. above 1%. This research focused on TiO_2 and ZnO nanocomposite membranes interaction with humic acid because of the lack of studies published on this particular topic.

Chapter 3 Materials and Methods

3.1 Materials

Polysulfone (PS) with a Mw of 60,000 was purchased from Scientific Polymer Products, Inc. (Ohio,USA). 1-Methyl-2-pyrrolidionone (NMP) was procured from Acros Organics Inc. (New Jersey, USA). Zinc oxide nano-powder (ZnO) (10-30 nm) was purchased from US research nanomaterials Inc. (USA). Titanium dioxide nano-powder (TiO₂) anatase form (30 nm) was purchased from US research nanomaterials Inc. (USA).

3.2 Preparation of Membranes

3.2.1 Preparation of Polysulfone Membranes

Virgin PS membranes were prepared via wet phase inversion method. First the polymer solution was prepared by dissolving 15 wt% of PS in NMP for 24 hours. The solution was stored in a tightly sealed glass container. Before casting, the solution was sonicated for 2 minutes in a UC-02 ultrasonic cleaner (medline scientific, UK) to allow any gas bubbles to escape. Casting was done manually on a glass plate at room temperature using a casting rod, Baker applicator, (TQC Inc. The Netherlands). The thickness of the cast solution was set to be 150 μm for all membranes, and it was allowed to dry for 30 seconds before being immersed in a de-ionized water bath that was kept at room temperature. The membranes were washed with deionized water and kept in de-ionized water bath for one day at room temperature to remove all traces of NMP. Membranes were stored in a tightly sealed container at approximately 4 C°

3.2.2 Preparation of Nanocomposite Polysulfone Membranes

The nanocomposite-polysulfone membranes were fabricated via wet phase inversion. 1 wt%, 2wt%, 3 wt% and 4 wt% nanoparticles were used to prepare the nanocomposite-polysulfone casting solution. The choice of this series was based on permeability of pure water (PWP) reported in the literature. Where a high PWP values were obtained by using this series of weights for both ZnO and TiO₂ (82,86).

First, nanoparticles and PS were dissolved separately in equal amounts of NMP and stirred for one day. After stirring for one day the nanoparticles were sonicated in UC-02 ultrasonic cleaner (medline scientific, UK) for 30 minutes. Then the sonicated solution was added to the PS solution and stirred for three hours. The solution nanoparticles-PS solution was then sonicated in UC-02 ultrasonic cleaner (medline scientific, UK) for 30 minutes. The casting was carried out by the same procedure carried above. Membranes were stored in a tightly sealed container at approximately 4 C°.

3.3 Membranes Characterization and Analysis

3.3.1 Scanning Electron Microscopy

Membranes SEM images were recorded using Quanta 450 FEG Environmental Scanning Electron Microscope (ESEM) (FEI, USA). The membranes were dried and fractured under liquid nitrogen prior to imaging or sliced using microtoming. The membranes were mounted aluminum stubs using carbon paint and coated with gold sputter (Q150R Rotary-Pumped Sputter Coater/Carbon Coater, Quorum technologies, UK)

3.4 Filtration Studies

The prepared membranes were tested for pre-compaction effect, water flux, and pure water permeability and fouling rate. All these tests were carried out using dead-end filtration cell (HP4750 stirred cell, sterlitech Inc., USA). The membranes were cut into round coupons 4.9 cm in diameter. The permeate mass was collected on a balance and the

weight was recorded by data acquisition system. The weight and time data was used to calculate membrane flux.

Membranes were first tested for pre-compaction by applying 5 bar pressure until 200 ml of permeate were collected. The pre-compaction flux was obtained from the slope of time versus weight. After determining the effect of pre-compaction, Water flux (J_w) was obtained. A pressure of 3 bar was applied on the membrane until 200 ml permeate were collected. Water flux was obtained from the slope of time versus weight. Pure water permeability (PWP) was obtained from the following equation:

$$PWP = \frac{J_w}{\Delta P}$$

The fouling rate was determined by filtrating 250 ml at concentration of 15 ppm humic acid. To minimize the concentration polarization effect i.e. homogenize the solution within the cell. A stirrer was used to stir the solution at 300 rpm. The stirrer was raised from the surface of the membrane to avoid mechanical friction or tearing of the membrane.

Humic acid was chosen as a model foulant because it is one of the most abundant foulants found in water. The filtration experiments were carried out at 3 bar pressure. And flux was calculated from the slope of time versus weight. The decay in flux was calculated as the ratio of the final flux to the initial flux. The concentration of humic acid in the filtrate was obtained using UV-Vis (Shimadzu, USA) absorbance at λ 283 nm. A linear relationship was found between HA concentration and absorbance at λ 283 nm, and is provided in Appendix A.

Fouling recovery ratio (FRR) was used to indicate membranes cleanability and anti-fouling properties. After fouling, membranes were tested for water permeation without stirring. FRR is calculated based on Eq. 2

$$FRR = \frac{\text{Water Flux After Fouling}}{\text{Water Flux Before Fouling}} \quad (2)$$

All experiments were carried out at room temperature.

3.5 Static Adsorption

Static adsorption was carried out to estimate the membranes affinity to HA. The membranes were cut into round coupons 4.9 cm in diameter. The coupons were dried and weighed then placed in vials containing 25 ml of 15 ppm HA solution. They remained in vials for 5 days, after which they were dried and weighed again. The difference between the initial and final weight was considered due to HA adsorption on the surface.

3.6 Membrane Pore Size, Porosity and Number of Pores

Polyethyleneglycol (PEG) with various molecular weights ranging from 1500 to 100,000 g/mol were used to obtain rejection data for membranes. PEG diameter was used to determine the mean pore diameter of membranes. The diameter of PEG was approximated using stokes diameter relationship (59,90):

$$d = 33.46 \times Mw^{.557} \times 10^{-10} \quad (3)$$

Where d is stokes diameter by (cm), Mw is the molecular weight of PEG (g/mol). The rejection of PEG was determined using chemical oxygen demand (COD) colorimeter (camlab,UK) . PEG rejection data was obtained at 3 bar, and after each run the membranes were flushed with pure water.

Stokes diameter and rejection data were plotted on a log-normal graph (found in Appendix B). Membranes mean pore size is the diameter which is equivalent to 50% rejection (90). The geometric standard is the ratio between stokes diameter at 84.13% rejection and the mean pore size (59,91). Geometric standard deviation is equal to the standard deviation because interactions between solute and pore sizes can be ignored.

Pore size distribution is expressed using probability density function (92):

$$\frac{df(d_p)}{d(d_p)} = \frac{1}{d_p \ln \sigma_p \sqrt{2\pi}} \exp\left(-\frac{(\ln d_p - \ln \mu_p)^2}{2 (\ln \sigma_p)^2}\right) \quad (4)$$

Where $f(d_p)$ is the fraction of pores with a given pore diameter (d_p), σ_p is the geometric standard deviation and μ_p is the mean pore diameter. The fraction of pores is presented in appendix B. The total pore numbers is calculated as (90):

$$N = \frac{128J\mu l}{P\pi \sum f(d_p) d_p^4} \quad (5)$$

Where (l) is the thickness layer of membranes, and it is set to equal 200 nm (90–92). P is pressure (bar), J is flux (L/m².hr) and μ is solution viscosity (Pa.s). Porosity (ϵ) is defined as the void fraction in a membrane i.e. the area of pores to the total surface area and it is defined as:

$$\epsilon = \frac{N\pi \sum f(d_p) d_p^2}{4} \quad (6)$$

Results and discussion is outlined in the following chapters.

Chapter 4: Effect of ZnO nanoparticles as additive on the performance and formation of polysulfone membranes fabricated via phase inversion.

ZnO nanoparticles (NP's) are used in a wide range of applications from toothpastes and sunscreens to solar-cells and LCDs (89). ZnO are known to have excellent chemical and mechanical properties alongside its hydrophilic nature (81). ZnO NP's are anti-bacterial, with excellent chemical electrical and mechanical properties (81,86,93). The hydrophilic nature of ZnO NP's, alongside their large surface area available for interaction as well as their commercial availability makes ZnO NP's an attractive candidate for modifying membranes.

Few studies have been reported on the incorporation of ZnO NP's in PES and PS membranes. These studies showed that such nanocomposite membranes exhibited an increase in pure water flux with increasing ZnO concentration (24,86). However, the interaction with natural organic matter was performed on low ZnO concentrations up to 0.5% wt (86). The study observed an increase in anti-fouling properties of membranes by 23%, when ZnO loading was 0.5% (86).

This current study was motivated by the published work on ZnO-nanocomposite membranes. This research is an attempt to further explore the behavior of these nanocomposite membranes over a wider range of NP concentrations. The focus of the study was the interaction between natural organic matter (humic acid) and the membrane. It was hypothesized that the expected increase in water flux for ZnO-nanocomposite membranes coupled with ZnO hydrophilic nature will help mitigate fouling.

4.1 Results and Discussion

Fabrication of ZnO-nanocomposite membranes aimed at improving water permeability and mitigating fouling. ZnO-nanocomposite membranes were expected to have an improved mechanical strength i.e. lower flux loss upon operation. The following discussion details the permeability of ZnO-nanocomposite membranes and their interaction with the foulant.

4.1.1 Pure Water Permeation

Pure water flux is defined as the volume of permeate (filtrate) collected per unit area per time(94). Pure water flux is used as a “baseline” for membranes performance (95). A higher pure water flux is desired quality in membranes, since it can be used to indicate hydrophilicity of membranes surfaces (86). The increase in hydrophilicity of membranes surface means a lower affinity of membranes to be fouled by hydrophobic foulants e.g. natural organic matter (NOM) (35). ZnO was added to polysulfone to increase the hydrophilicity of membranes and improved pure water flux. The water flux of fresh membranes was recorded with time. Examples of such results are shown in Figure 19.

A significant enhancement in the flux for higher ZnO concentrations is depicted in Figure 19. A significant jump in flux occurs from 1% membranes and 2% membranes. The increase in pure water permeability (PWP) in membranes is a good indication to the increase of hydrophilicity of membranes (86). But it might also be a result of the change in membrane surface morphology, or the cross sectional structure of membranes (5,95,96).

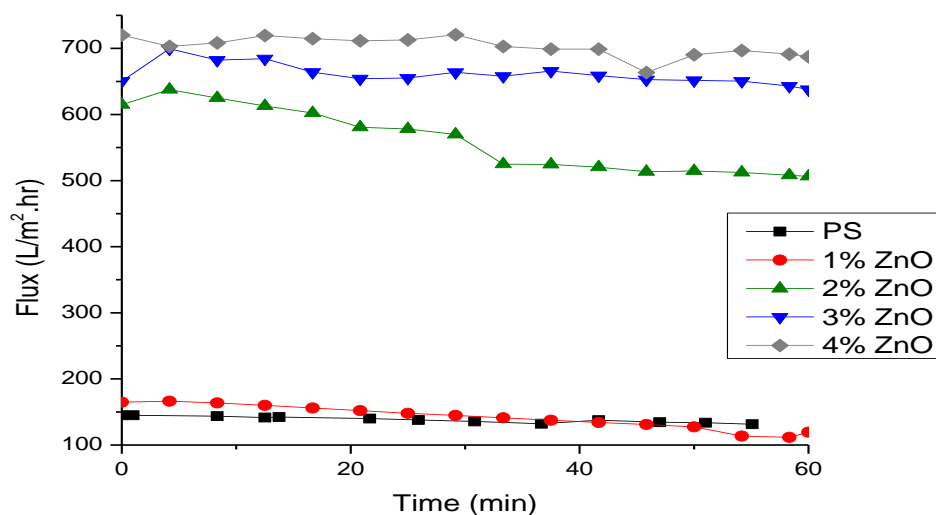


Figure 19 pure water flux of ZnO-nanocomposite membranes with different ZnO concentrations in the casting solution. Each line presents the average of four samples. Membranes were tested using distilled water at 3 bar.

Pure water permeation (PWP) is summarized and presented in Figure 20. It can be clearly seen that there is a significant jump in the PWP value between the 1 and 2 wt% samples. As the concentration of ZnO increases, PWP remains almost the same with no significant changes.

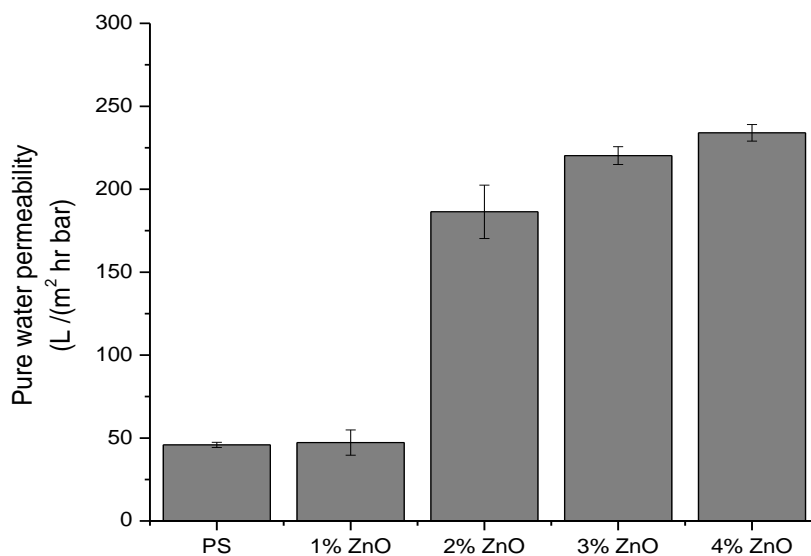


Figure 20 Pure water flux of ZnO-nanocomposite membranes with different ZnO concentrations in the casting solution. Membranes were tested using distilled water at 3 bar. Each bar represents the average of four samples

4.1.2 Membrane surface morphology and structure

Increase in PWP might indicate that the membranes are more hydrophilic, but it is not the only factor determining the water flux. PWP was also found to be directly related to membranes surface roughness (54,97). A rougher membrane surface was found to be more porous one (96). The relationship between membranes surface roughness and porosity is due to the presence of “valleys”, which contribute to the increase in surface roughness parameters when tested using AFM (96). The relationship between membrane surface porosity and PWP is confirmed using modified Hagen-Poiseuille relationship (8):

$$PWP = \frac{\varepsilon d^2}{32 \mu l} \quad (1)$$

Where ε is porosity (void fraction) on membrane surface, d is the mean pore diameter of membranes, μ is the viscosity of water and l is the thickness of the active layer. In other words, increasing the number of pores and/or the diameter of pores increases PWP, and it is reflected as an increased roughness in membrane surface (8,54,96).

In order to investigate the effect porosity and mean pore size on PWP, MWCO data was used to determine mean pore size and porosity. Table 3 shows the calculated porosity values of ZnO-nanocomposite membranes.

Table 3 porosity (ε), mean pore diameter (μ_p), and geometric standard deviation (σ_p) of ZnO nanocomposite membranes

<i>Membrane</i>	<i>μ_p (μm)</i>	<i>ε (%)</i>	<i>σ_p (nm)</i>
<i>PS</i>	2.4	1.2	4
<i>1% ZnO</i>	0.52	1.5	2
<i>4% ZnO</i>	0.57	7.3	2

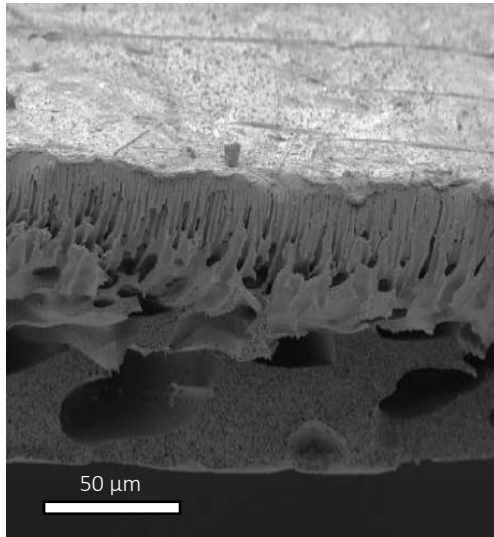
The porosity of ZnO-nanocomposite membranes increases with increasing ZnO concentration (Table 3). This means that the increase in PWP for ZnO-nanocomposite

membranes is a result of increasing membranes surface porosity with increasing ZnO concentration in the membrane. The geometric standard deviation reported in Table 3 is similar to the geometric standard deviation reported for ultrafiltration membranes in literature (10)- (11).

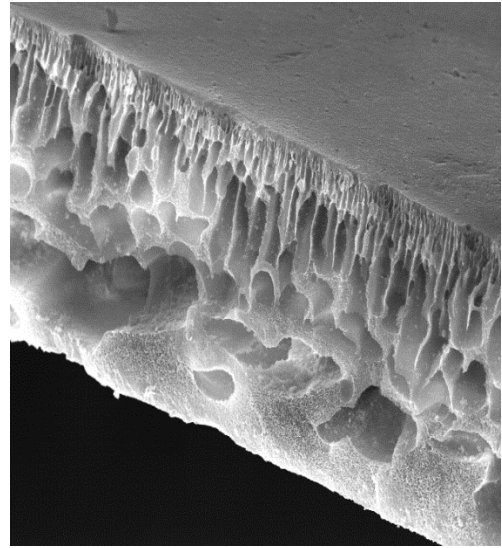
The increase in ZnO-membranes porosity as ZnO concentration increases indicates a possible change in membrane internal structure. The internal structure of membranes consists of a narrow porous structure (finger-like) followed by enlarged cavities in the permeate side of the membrane (macrovoids) (18)- (100).

Structure of different membranes with different ZnO loadings is shown in Figure 21. The cross sectional structure of ZnO-nanocomposite membranes seems to be a function of ZnO loading in the membranes. At higher ZnO, the size of macrovoids increases which contributes to the mechanical instability of membranes (5). Furthermore, the thickness of the active layer decreases with increasing the concentration of ZnO in the membranes.

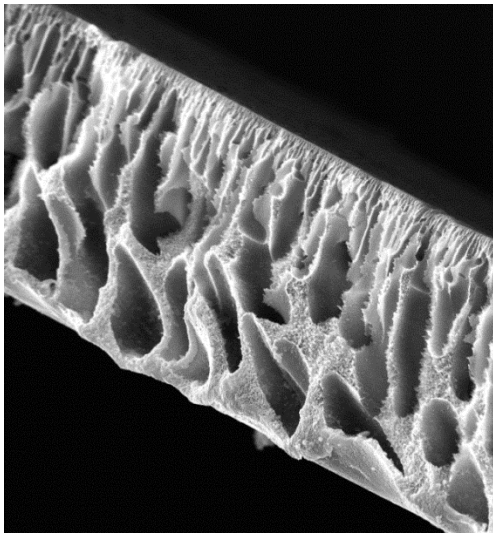
The final membranes structure (finger like or sponge like) is controlled by the rate of diffusion of solvent (J_{NMP}) from the organic phase and into the aqueous phase and the rate of diffusion of the non-solvent (J_{water}) from the aqueous phase to the organic phase (5,100). Macrovoids are formed when rate of J_{water} exceeds that of J_{NMP} , in other words if the polymer film has a higher affinity to the non-solvent (5). The increased formation of macrovoids with ZnO loading in nanocomposite membranes can be attributed to two factors. First, the increase in J_{water} due to the presence of hydrophilic ZnO in the polymer casting film. Second is the hindrance effect nanoparticles have on the outward diffusion of solvent from the polymer film (81,86). As a result, the presence of NP's is expected to favor macrovoids formation.



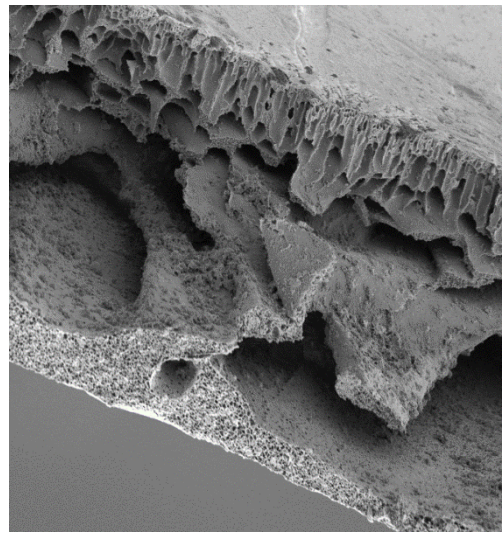
(a)



(b)



(c)



(d)

Figure 21. SEM images of cross sections of membranes with different ZnO concentrations in the casting solution: (a) PS, (b) 1% ZnO, (c) 2% ZnO, (d) 4% ZnO.

ZnO-nanocomposite membranes clearly have an increased number of macrovoids. The increase in macrovoids formation is what causes the decrease in active layer thickness and the fabrication of finer pores for ZnO-nanocomposite membranes (Table 3). During the initial stages of phase inversion, the more hydrophilic ZnO-nanocomposite membranes have a higher rate of J_{water} and J_{NMP} exchange i.e. demixing is instantaneous. This causes the formation of macrovoids. As the exchange process continues, the formed macrovoids are surrounded by a thicker i.e. more concentrated polymer solution (101).

The combined effect of a thicker polymer solution as well as the hindrance effect of ZnO NP's slows J_{NMP} (86,100,102). This causes the formation of a denser active layer with finer pores (26,101).

The increase in macrovoids for ZnO-nanocomposite membranes might aggravate flux loss during initial stages of operation i.e. compaction (103). Compaction is defined as decay in water flux due to deformation in membranes structure (103). Deformation in membrane structure is mainly caused by macrovoids collapsing under pressure, which hinders water movement and lowers flux as operation proceeds (26).

4.1.3 Compaction of Membranes

Based on SEM cross sectional images (Figure 21) and the high increase in PWP (Figure 19) for ZnO-nanocomposite membranes, one might expect that the compaction of such highly permeable membrane would increase significantly as well. However, this was not the case as seen in Figure 22. Flux loss shows some increase as ZnO concentration increases, however, this increase was moderate compared to the observed 5 fold increase in PWP. For example, in Figure 22, except for the highest ZnO concentration sample (4 wt%), the flux loss was comparable among all samples (within experimental variation). This might indicate the collapse of larger macrovoids in the structure, but it might also be the direct result of higher initial flux (104).

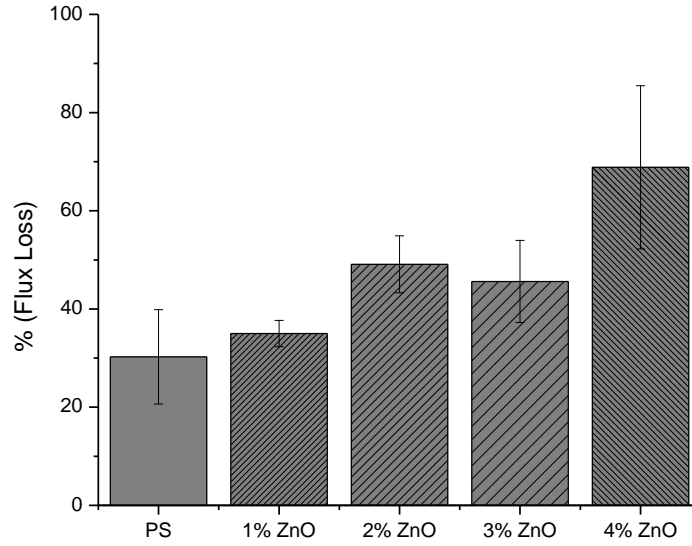


Figure 22 Effect of different ZnO concentrations on the flux loss of nanocomposite membranes. Flux was measured using distilled water at 5 bar. Each bar represents the average of 4 samples.

The dynamics of the flux decline were found to be highly dependent on ZnO concentration. The change in flux with time can be described using (104):

$$\frac{J}{J_o} = \left(\frac{t}{t_o} \right)^{-n} \quad (1)$$

Where J is the final flux, J_o is the initial flux, t_o is characteristic time and t is the final time, n is the compaction exponent and it is used to describe the compliance of the membrane to pressure application (104). Figure 23 shows the results of fitting flux data to Eq. (1) for the different membranes. It is clear that the exponent value is a function of ZnO loading in the membrane matrix. Sample with higher ZnO loadings have high exponent (faster response to pressure) than those with lower loadings. The values of the compaction exponent for the 3% and 4% membrane samples exceed those reported in literature (n is typically <0.1) (104).

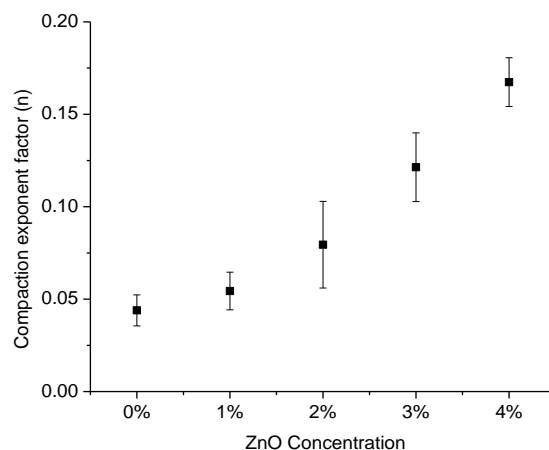


Figure 23. Effect of ZnO concentrations on -compaction exponent nanocomposite membranes. Membranes were tested for 1 hour using deionized water at 5 bar. Each point represents the average of 4samples.

The faster response indicates increased elasticity of the membrane which can be attributed to the presence of the macrovoids. The faster response could also be due to the increase in membranes porosity as ZnO loading increases (Table 3) (105). Compliance of porous membranes to pressure application has been found to be directly related to membranes porosity (106). ZnO NP's might also contribute to flux loss during initial stages of operation, if they are present within the membrane pores. Since ZnO NP's might block certain pores or contribute to the overall flow resistance of water through ZnO-nanocomposite membranes pores.

TEM was used to investigate the dispersion of ZnO NP's within the membrane as shown in Figure 24. The images show a tendency for the ZnO NP's to accumulate at the pore surface or within the pores. This indicates the migration of ZnO takes place during phase inversion since ZnO are hydrophilic in nature. The extent to which ZnO NP's migrate seems to depend on its concentration. For the 2 wt% sample, the nanoparticles seems to migrate further into the pores forming agglomerates that are entrapped within the membranes pores. At 4 wt%, the NP's are more concentrated at the pore surface.

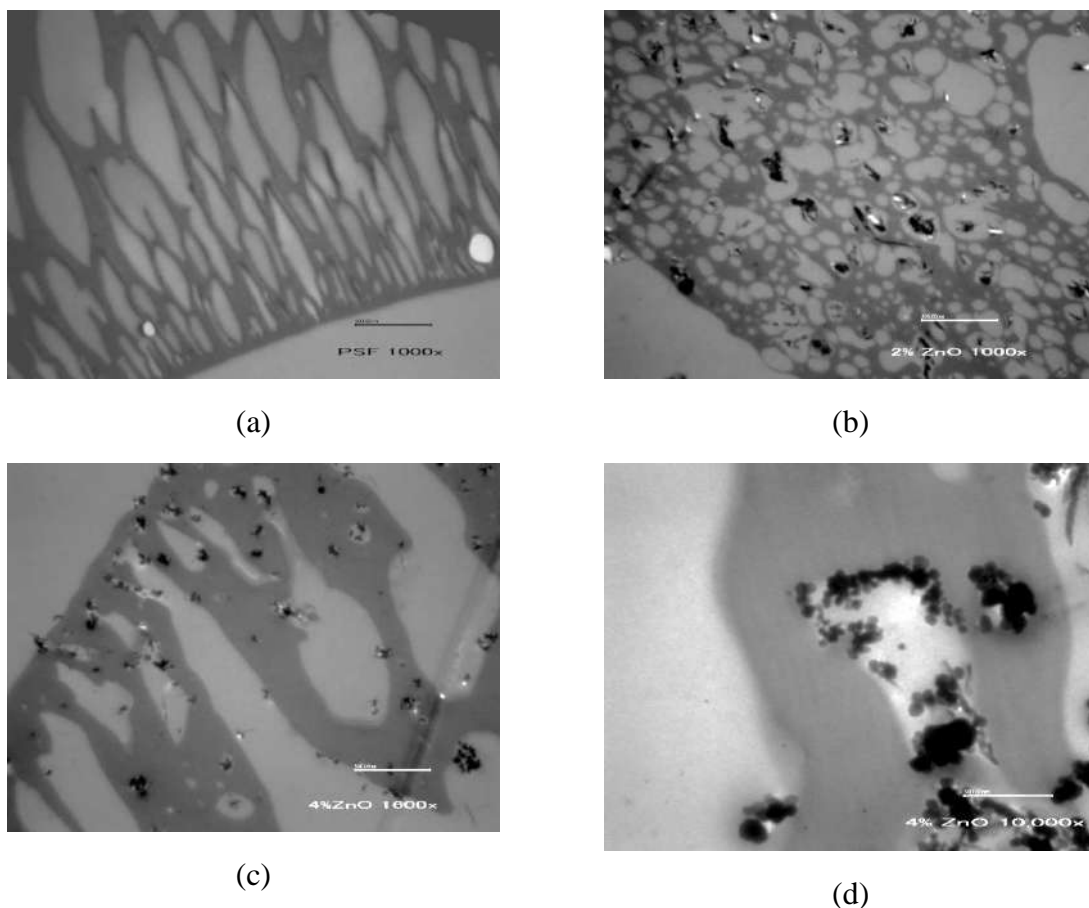


Figure 24. TEM images of different membranes: (a) PS, (b) 2% ZnO (c) and (d) 4% ZnO. Scale bars are 500 nm.

From this section one can gather that addition of ZnO NP's has a positive effect on membranes water flux. The increase in water flux might be due to an increase in the surface hydrophilicity of the membrane or change in membrane surface morphology.

4.1.4 Fouling and cleanability

The addition of the hydrophilic ZnO NP's to the hydrophobic PS membrane was meant to improve membranes performance, i.e. increase flux and mitigate fouling. To test the fouling performance of the synthesis membranes, experiments with HA as model foulants were performed. Samples of flux data recorded during HA filtration experiments is shown in Figure 25. The initial flux decline was more severe at higher ZnO concentrations.

The results are shown in Figure 25 and show that 2%, 3% and 4% had an initial high rate of flux decline than 0% and 1% membranes. However, as the experiment proceeded 2%,

3% and 4% membranes showed a lower rate of flux decline. The high initial decline in flux for 2%-4% membranes might be due to the higher permeation drag caused by the increase in flux (54).

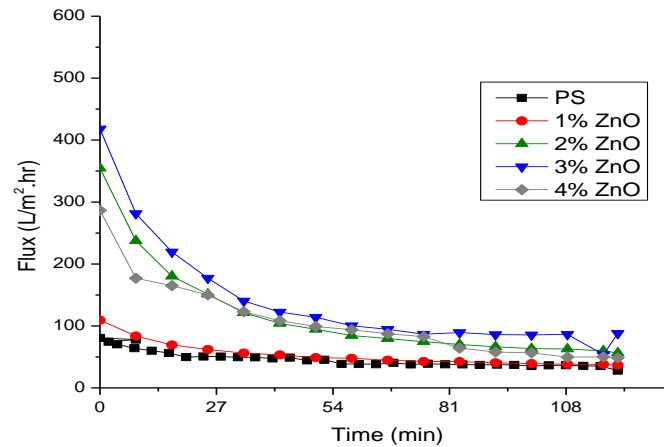


Figure 25. Effect of ZnO concentration on flux during HA filtration. Membranes were tested using 15 ppm HA at 3 bar. Each curve represents an average of 4 membrane samples.

The decline in flux for 2%-4% membranes is severe compared to 0% and 1% membranes. This is an interesting result because despite being more hydrophilic, these membranes show an “affinity” to fouling by humic acid (Figure 26). To understand this behavior, HA-ZnO interactions must be considered.

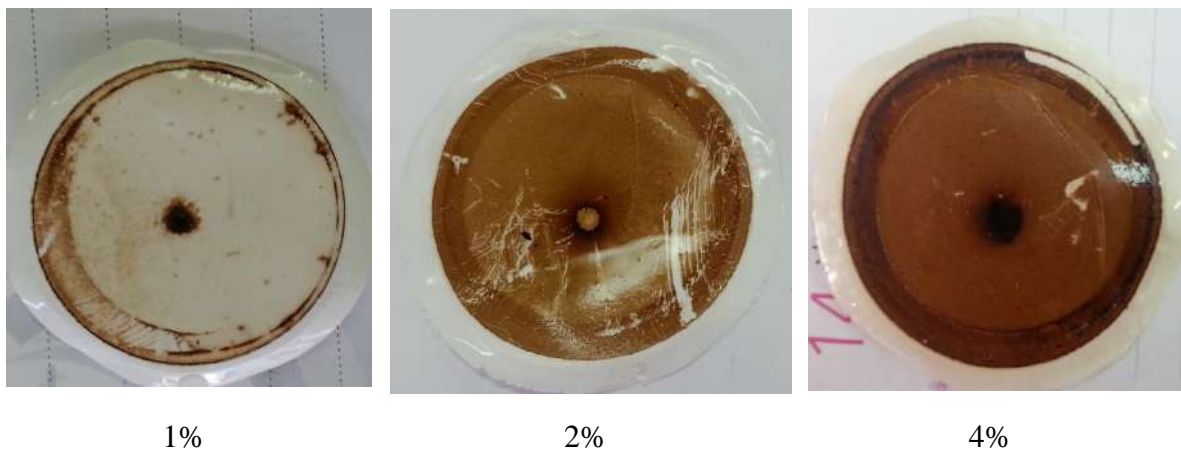


Figure 26. Appearance of different membranes after HA fouling experiments.

The affinity of membranes containing ZnO towards HA can be explained by the tendency of HA to adsorb on ZnO surface (107). HA interacts and adsorbs on the surface of ZnO via two methods, ligand exchange and electrostatic interaction (107). The large surface area of ZnO allows the phenolic COOH and OH groups in HA to form ligand exchange (107). Another possible reason behind the severe fouling of ZnO-nanocomposite membranes is the release of Zn^{+2} cations from ZnO NP's (88). If Zn^{+2} is present in water, it will bind with the negatively charged COOH groups found in HA making it more spherical in shape (51). This in turn will cause the HA to form denser, more compact layer on top of the membrane surface, as seen in Figure 26 (51,54).

The release of Zn^{+2} cations from ZnO-nanocomposite membranes was tested using inductively coupled plasma (ICP). The test was carried out for 0% membrane and 4% membranes. Where a sample of membranes (of similar size) were kept in 25 g of ultrapure water for one day. 20 g sample of water was then centrifuged for 25 minutes and 1 ml was taken from the surface. The sample was then digested with 9 ml of 1% HNO_3 .

The release of Zn^{+2} cations from ZnO-nanocomposite membranes was confirmed from the ICP analysis. Where (6680 ppb) were found to be present in 1 ml of water. Compared to a trace amount of Zn^{+2} found for 0% membranes, which is most likely due to contamination. The results of the ICP analysis that both chemical and physical factors contribute to the exacerbation of fouling. In other words, addition of ZnO NP's as a modifying agent should be avoided. Moreover, the release of Zn^{+2} cations from ZnO-nanocomposite membranes poses an environmental threat(88). Especially to aquatic life forms such as algae and fish (88).

The affinity of ZnO-nanocomposite membranes to be fouled was tested with static adsorption tests. Static adsorption has the advantage of representing the interaction

between membrane surface and foulant in the absence of other driving forces, i.e. pressure (108). The percentage of weight increase after static adsorption test for different membrane samples is shown in Figure 27. Membranes containing ZnO had a higher affinity to HA than 0% sample. However, there is no clear pattern regarding HA interaction with different ZnO loading in membranes.

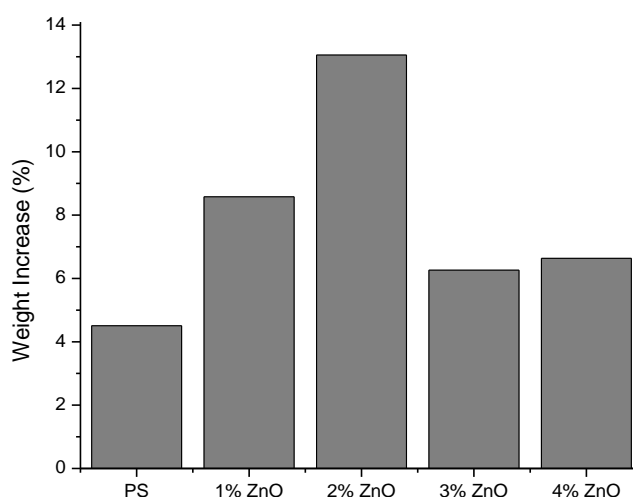


Figure 27 Effect of different concentrations of ZnO-nanocomposite membranes on percentage of weight increase during static adsorption test. Static adsorption test was carried out using 15 ppm HA at room temperature.

A good indicator of membrane antifouling properties and cleanability is the fouling recovery ratio (FRR) (16). FRR of ZnO-nanocomposite membranes is shown in Figure 28. 0% and 1% membranes had similar FRR ratio within the experimental error margin. However, as ZnO concentration in the casting solution increases, FRR decreases. This could be a direct result of HA affinity to ZnO NP's in the nanocomposite membrane. Also, cleaning of ZnO-nanocomposite membranes might be more difficult than that of PS membranes. Since ZnO-nanocomposite membranes have more porous surface i.e. rougher surface (Table 3) and HA might be adsorbed on surface of ZnO NP's (54,107).

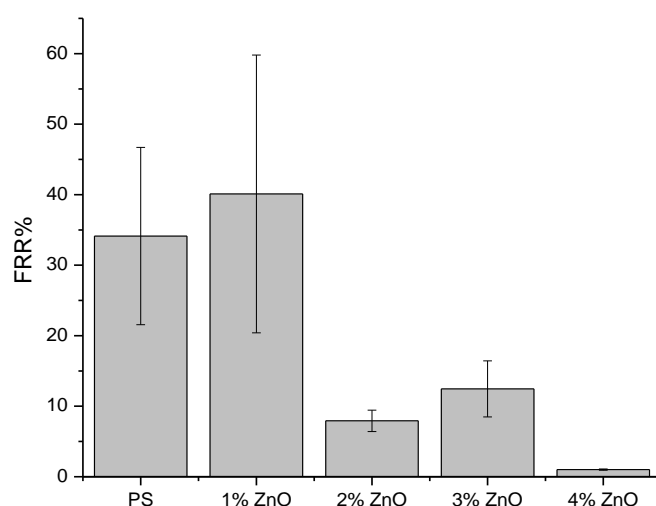


Figure 28. Flux recovery ration for different HA-fouled membranes. Membranes were tested using deionized water at 3 bar and no stirring. Each bar represents the average of at least 2 samples.

4.2 Conclusions

The fabricated ZnO-nanocomposite membranes exhibited an improved PWP. The improvement in PWP was found to be a function of ZnO loading. The increase in PWP could be due to increase in hydrophilicity of membranes and to increase in membranes surface porosity. Membranes surface porosity was found to increase with increasing ZnO loading in the membranes, but the mean pore diameter decreased with increasing ZnO loading in the membranes. ZnO-nanocomposite membranes internal structure was found to have larger macrovoids, but thinner active layer. The presence of macrovoids caused the ZnO-nanocomposite membranes to be more prone to compaction i.e. more sensitive to applied pressure. The increase in ZnO-nanocomposite membranes to applied pressure could be also due to the increase in porosity and to the presence of ZnO NP's in the pores of fabricated membrane.

ZnO-nanocomposite membranes exhibited increased affinity towards humic acid. The decline in flux detected for ZnO-nanocomposite membranes could be due to the

permeation drag caused by the higher initial flux. It could also be due to the adsorption of humic acid on ZnO NP's surface. The release of Zn^{+2} from ZnO-nanocomposite membranes contributes to increasing humic acid fouling and forming a denser more compact layer on the membrane surface.

Chapter 5: Effect of TiO₂ Nanoparticles As Additive on the Performance and Formation of Polysulfone Membranes Fabricated Via Phase Inversion.

Current applications of TiO₂ NP's are quite extensive and ranging from photo catalysis to biomedical applications (107). The commercial availability, stability hydrophilicity of TiO₂ NP's makes them an excellent choice as an additive for water purification (82). The use of TiO₂ NP's is considered challenging due to their larger surface area providing more space for interaction and therefore being harder to disperse (109). Nonetheless, the applications of TiO₂ NP's in membrane applications and water treatment is still looked at favorably and several techniques have been employed to help with TiO₂ dispersion i.e. modification of TiO₂ surface to reduce agglomeration (16,80) .

Rutile and anatase are the two crystalline phases of TiO₂ NP's. Anatase TiO₂ NP's have smaller diameter than that of rutile TiO₂ NP's, which increases the effectiveness of anatase TiO₂ NP's in water treatment applications (84). However, anatase TiO₂ NP's were reported to be more toxic when inhaled, they were also reported to be cytotoxic in mammalian cells (45,110). But it was reported that the toxicity of NP's if their size exceeds 30 nm is similar to that of their bulk counterparts (111). So in order to ensure the safety of water and to fabricate hydrophilic anti-fouling membranes anatase TiO₂ NP's with a size of 30 nm were used to for this research.

5.1 Results and Discussion

5.1.1 Pure Water Permeability

As was discussed in chapter 4, pure water flux is used as a “baseline” for membranes performance (95). TiO_2 -nanocomposite membranes were expected to have an increased pure water flux compared to polysulfone membranes i.e. 0% membranes. This expectation stems from the hydrophilic nature of TiO_2 NP's, which will cause an increase the hydrophilicity of membranes surface, as well as changing the membrane surface morphology and internal structure (5,86,95,96). The water flux of fresh membranes was recorded with time. Examples of such results are shown in Figure 29.

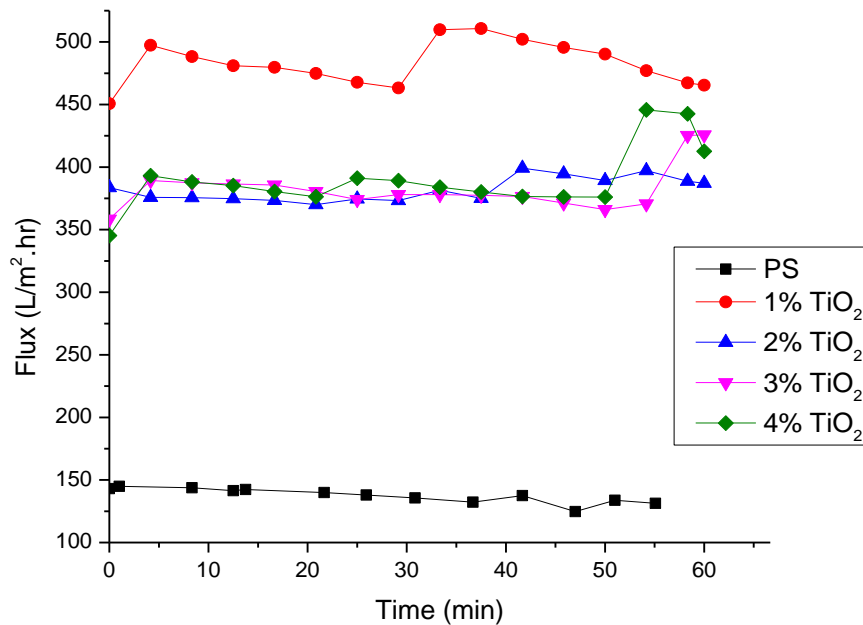


Figure 29 pure water flux of TiO_2 -nanocomposite membranes with different TiO_2 concentrations in the casting solution. Each line presents the average of four samples. Membranes were tested using distilled water at 3 bar.

Enhancement in flux for all TiO_2 -nanocomposite membranes is depicted in Figure 29. Water flux of 2%-4% membranes was almost the same. In Figure 29, a sudden increase in flux recorded for 1% TiO_2 -nanocomposite membranes. This is due to refilling the static

cell once permeate collected was 250 ml. The sudden increase in flux recorded might indicate that TiO₂-nanocomposite membranes are elastic i.e. not deformed permanently by the application of pressure.

Average pure water permeation (PWP) is summarized in Figure 30. TiO₂-nanocomposite membranes show an improved PWP for all tested TiO₂ NP's. However, there is no significant difference in PWP as the concentration of TiO₂ NP's increases.

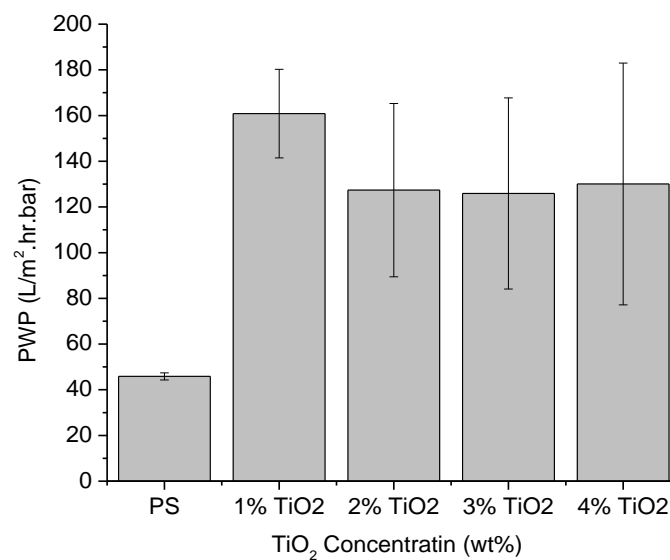


Figure 30. Effect of TiO₂ concentration on pure water permeation. PWP was measured using distilled water at 3 bars. Each bar represents the average of 4 samples.

ZnO-nanocomposite membranes had on average a higher PWP than that of TiO₂-nanocomposite membranes reported in Figure 30. The difference in PWP for ZnO-nanocomposite membranes and TiO₂-nanocomposite membranes could be due to a difference in membranes morphology i.e. surface porosity. The following section details the morphology and structure of TiO₂-nanocomposite membranes.

5.1.2 Membranes surface morphology and structure

As was discussed in chapter 4, pure water permeation depends on the porosity of membranes and the pore diameter. The dependency of flux on these parameters is

described using Hagen-Poiseuille relationship. Table 4 represents the porosity values of TiO₂-nanocomposite membranes.

Table 4 porosity (ϵ), mean pore diameter (μ_p), and geometric standard deviation (σ_p) of TiO₂ nanocomposite membranes

<i>Membrane</i>	<i>μ_p (μm)</i>	<i>ϵ (%)</i>	<i>σ_p (nm)</i>
PS	2.4	1.2	4
1% TiO₂	1.2	2.6	24
4% TiO₂	1.1	3.0	1

TiO₂-nanocomposite membranes have an increased porosity compared to that of 0% membrane. The increase in porosity might be responsible for the increase in PWP for TiO₂-nanocomposite membranes (Figure 30). However, TiO₂-nanocomposite membranes have lower porosity and larger mean pore diameter than that reported for ZnO-nanocomposite membranes. Which might help to explain the lower PWP values reported for TiO₂-nanocomposite membranes compared to ZnO-nanocomposite membranes.

Similar observations regarding membrane porosities were reported in the literature for PVDF-ZnO and PVDF- TiO₂ membranes. PVDF- TiO₂ membranes were reported to be smoother i.e. less porous surface than virgin PVDF membranes (19). On the other hand, the roughness i.e. surface porosity of PVDF-ZnO membranes was reported to have increased when ZnO concentration exceeded 0.005% (87). The decrease in PVDF- TiO₂ membranes porosity was attributed to the association of TiO₂ and PVDF, where hydrogen bonds are supposedly formed between PVDF fluorine and TiO₂ oxygen (19). If similar hydrogen bonding is formed between TiO₂ and PS, then fabricated TiO₂-nanocomposite membranes would have a denser skin layer than ZnO-nanocomposite membranes. The cross sectional structure of TiO₂-nanocomposite membranes was studied using SEM and is presented in Figure 31.

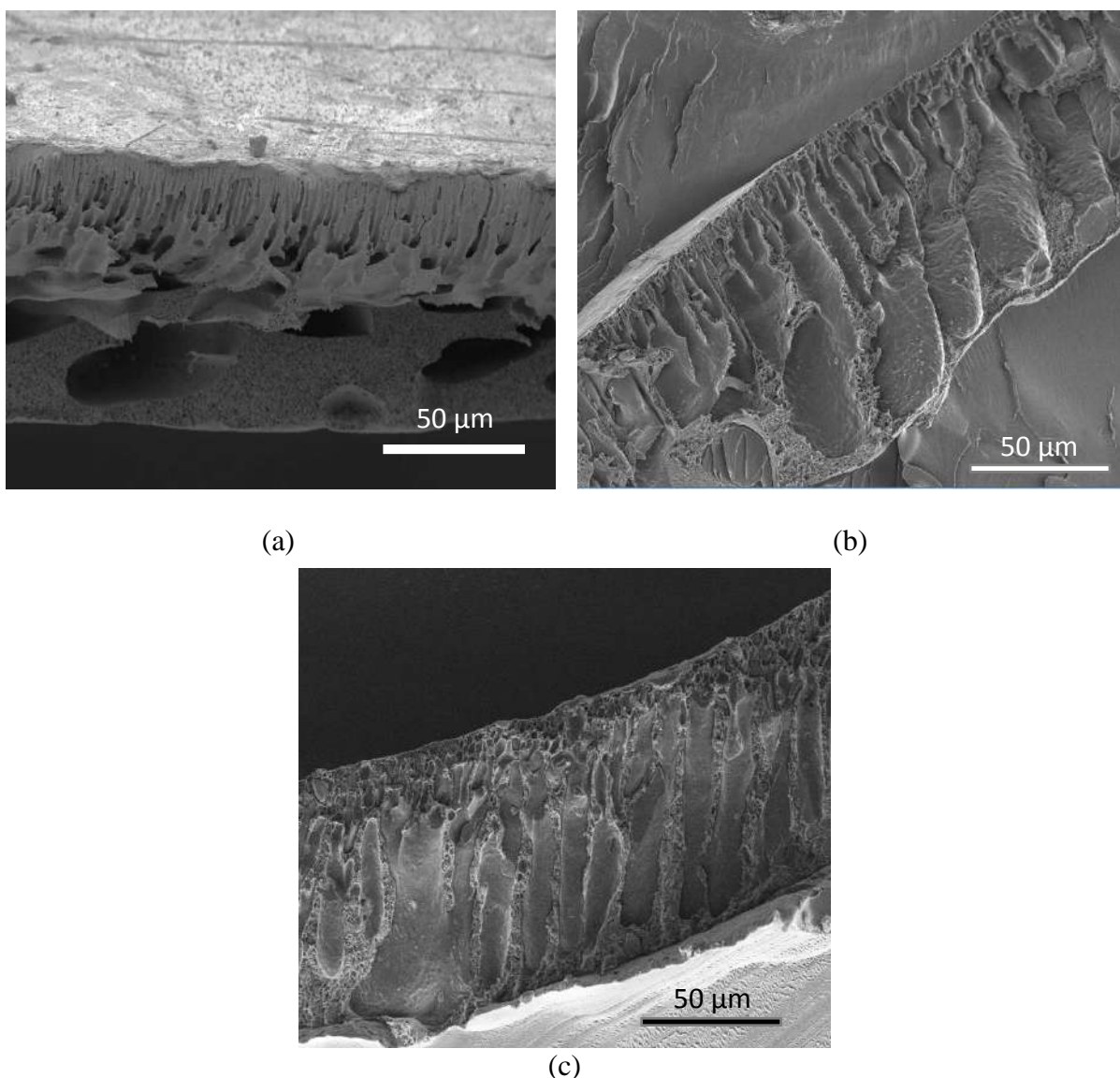


Figure 31. SEM images of cross sections of TiO_2 -nanocomposite membranes: (a) PS (b) 2% TiO_2 and (c) 4% TiO_2 in the casting solution.

TiO_2 concentration of 2% and 4% membranes presented in Figure 31 seem to have a similar structure. Despite not having a clear view due to microtoming, the size of macrovoids of TiO_2 -nanocomposite membranes is much smaller than ZnO -nanocomposite membranes. This might indicate that PS- TiO_2 casting solution is more viscous than PS-Zn casting solution. This hypothesis is further fortified by the decreased porosity of TiO_2 -nanocomposite membranes compared to ZnO -nanocomposite membranes (Table 4) (82).

The increase in viscosity of PS- TiO_2 casting solution prevents the free movement of water molecules during phase inversion (5,82). Increase in PS- TiO_2 casting viscosity might be

due to polymeric (PS) chains adsorption on TiO_2 surface due to the high specific surface area and energy of TiO_2 NP's (80,82). On the other hand, the presence of ZnO NP's propels water movement into the polymer film during phase inversion, which increases the porosity of membranes and enhances macrovoids formation (24,86). The structure of TiO_2 -nanocomposite membranes suggest that initial decline in flux i.e. compaction might be mitigated. The following section details the behavior of membranes during initial stages of operation.

5.1.3 Compaction of membranes

Compaction of TiO_2 -nanocomposite membranes will give further insight into the membranes strength (103). Figure 32 depicts the loss of flux due to compaction for synthesized membranes with different TiO_2 concentrations. 1% membrane showed a higher flux decline than 0% membranes, this might be due to the higher initial flux of 1% membranes. Compaction of TiO_2 -nanocomposite decreased as TiO_2 concentration increased up to 3%. This might indicate suppression of macrovoids as TiO_2 concentration increases due to increase in viscosity (82). At TiO_2 concentration of 4% membranes suffered an increase in flux decline.

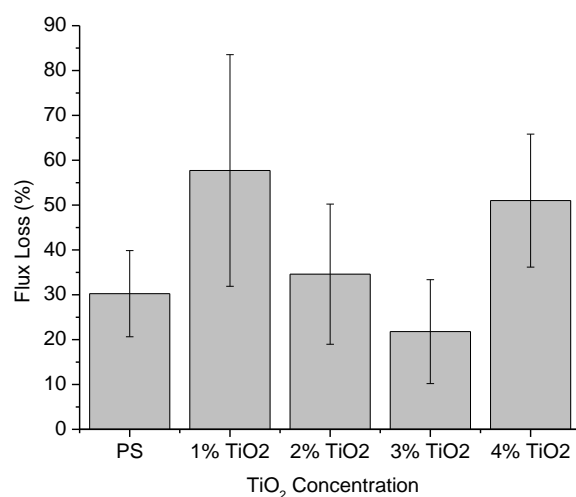


Figure 32. Effect of TiO_2 concentration on flux loss during compaction at 5 bars. Flux was measured using distilled water at 5 bar. Each bar represents the average of 4 samples.

The compaction of ZnO-nanocomposite membranes had a different trend than that of TiO₂-nanocomposite membranes. ZnO-nanocomposite membranes showed an increase in flux decline as the concentration of ZnO NP's increased. This was attributed to an increase in macrovoids formation and to an increase in ZnO-nanocomposite membranes surface porosity with increasing ZnO NP's concentration (105,106). Compared to TiO₂-nanocomposite membranes, 1% ZnO-nanocomposite membrane had a lower flux decline than that reported for 1% TiO₂-nanocomposite membranes. However, as the loading of ZnO NP's increases, the flux decline of ZnO-nanocomposite membranes surpasses that of TiO₂-nanocomposite membranes even within the experimental error range. This might be due to ZnO-nanocomposite membranes increase in porosity as ZnO loading increases. Both ZnO and TiO₂-nanocomposite membranes showed an increase in flux decline compared to 0% membranes, indicating an increase in porosity of nanocomposite membranes (106).

As mentioned in chapter 4, flux loss percentage is not an accurate depiction of membrane sensitivity to pressure. Since it was found that at higher initial flux membranes tend to have higher flux loss percentages (104). In order to eliminate the effect of initial flux, the pre-compaction exponent factor (-n) was calculated and is presented in Figure 33.

The pre-compaction exponent factor of 0%, 2% and 3% were similar ($-n \approx .04$). Indicating that 2% and 3% membranes are less sensitive to the application of pressure than 4% membranes. This could be due to the suppression of macrovoids formation. Despite the wide error bars of 1% membrane, it had highest pre-compaction exponent factor recorded ($-n \approx .12$). The increase in pre-exponent factor for 4% membranes could be related to an increase in 4% membranes surface porosity (112).

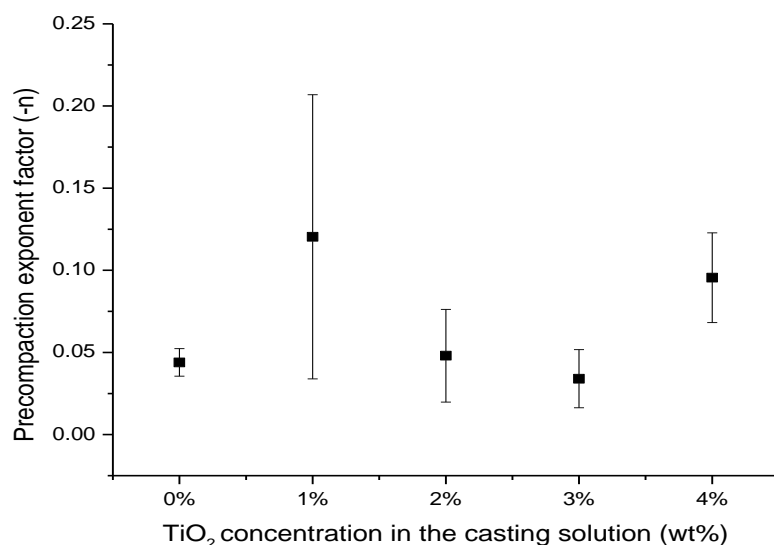


Figure 33 Effect of different TiO₂ concentrations in membranes on pre-compaction exponent factor and scatter for PS- TiO₂ nanocomposite membranes, each point is averaged over four samples.

Compared to ZnO-nanocomposite membranes, TiO₂-nanocomposite membranes are less sensitive to pressure application. 4 wt% TiO₂-nanocomposite membranes had a pre-compaction exponent factor of $-n \approx 0.09$. On the other hand, for 4 wt% ZnO-nanocomposite membranes pre-compaction exponent factor was ($-n \approx 0.17$), which was higher than the values reported in literature (104). Despite 1% TiO₂-nanocomposite membranes having an average higher pre-compaction factor, the large error bars makes it difficult to properly judge 1 wt% membrane behavior.

In order to obtain a better understanding of TiO₂-nanocomposite membranes internal structure, and to verify the proposed interaction between PS and TiO₂, TiO₂-nanocomposite membranes were imaged using TEM. Figure 34 shows the presence of agglomerates in the 2 wt% and 4 wt% membrane samples, which is expected due to TiO₂ NP's high surface energy (109). The presence of agglomerates was also detected for ZnO, however the size of the agglomerates of TiO₂ NP's was much larger than that of ZnO.

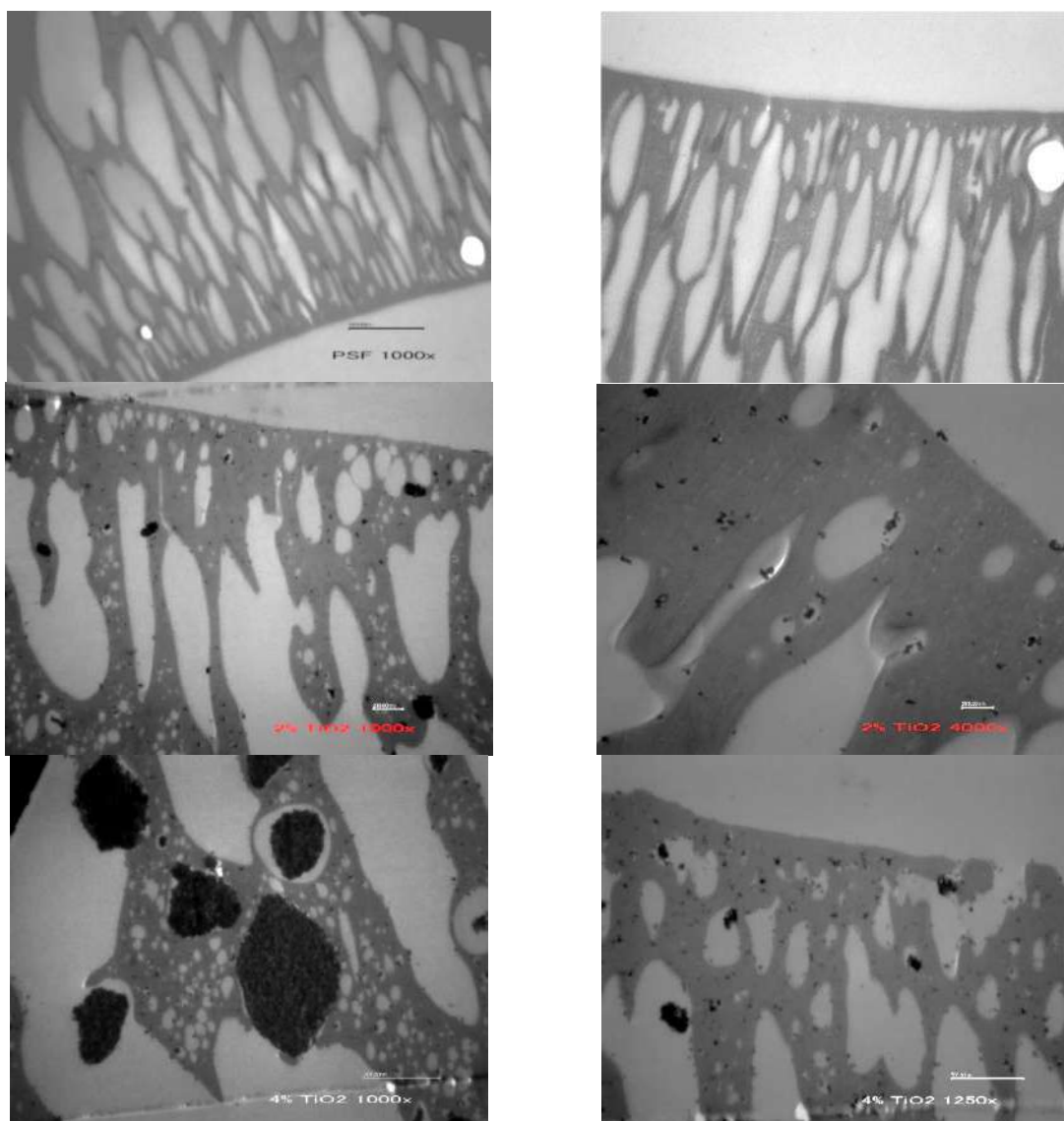


Figure 34 TEM images of different membrane samples at PS, 2% TiO₂ and 4% TiO₂ concentration.

The pore structure of TiO₂-nanocomposite membranes is more round and sponge like at 2 wt% and 4 wt% as opposed to elongated and finger like at 0%. Change in pore shape might cause a change in water permeation. Furthermore, the presence of hydrophilic TiO₂ inside and around the pore walls might promote water to pass through the membranes, hence increasing water permeation (Figure 30).

TiO₂ presence inside the pores of the membranes is shown in Figure 34. This could be due to the migration of nanoparticles to the pores during phase inversion. The 4 wt% sample have a higher concentration of TiO₂ NP's in and around the pore walls, which may hinder

water movement during filtration or block the pores causing a higher decrease in flux. Both the 2 wt% and 4 wt% samples show high presence of TiO₂ within the polymer matrix, which might be due to the adsorption of PS on TiO₂ surface (80,82). A property that was not observed for PS-ZnO membranes. The high concentration of TiO₂ nanoparticles inside the polymer matrix and not in the pores might mitigate fouling. The following section discusses the anti-fouling properties of TiO₂-nanocomposite membranes.

5.1.2 Fouling and cleanability

Incorporation of TiO₂ NP's was intended to improve the anti-fouling properties of PS membranes. Fouling was tested using 15 ppm HA under pressure of 3 bar. The performance of TiO₂ nanocomposite membranes is depicted in Figure 35. The final average flux of all TiO₂ membranes is almost 100 L/m².hr exceeding that of pristine PS membranes. However, the flux decline is still severe and cannot be expressed properly without being normalized. Relative flux of membranes ($RF = J/J_{PWP}$) is shown in Figure 36, which is a better indication to the membrane affinity to foulant, because RF will normalize the membranes performance with respect to membranes initial flux.

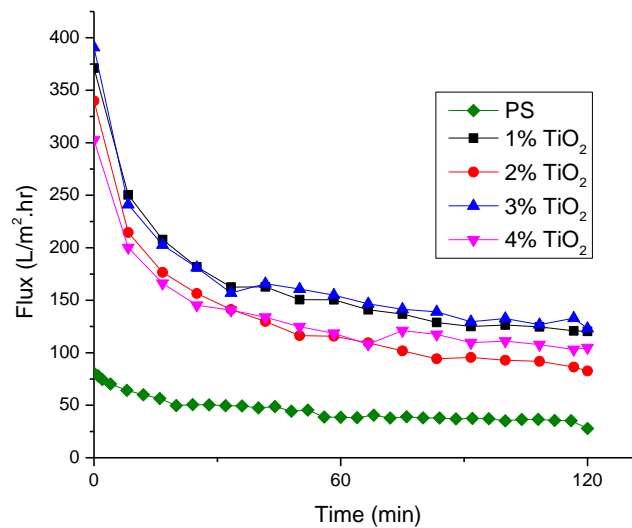


Figure 35 Effect of ZnO concentration on flux during HA filtration. Membranes were tested using 15 ppm HA at 3 bar. Each curve represents an average of 4 membrane samples

The initial RF was higher for all TiO₂ nanocomposite samples compared to the PS samples. The rate of flux decline of TiO₂ nanocomposite membranes is lower than that of 0% membrane. Indicating that TiO₂ nanocomposite membranes have lower affinity to be fouled even when the permeation drag increased. A maximum RF was recorded for 3% TiO₂ membranes, which could be due to the increase in membranes hydrophilicity.

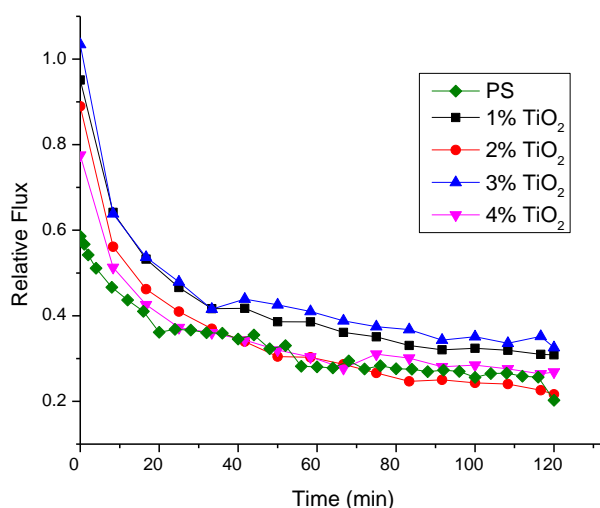


Figure 36. Effect of TiO₂ concentration on the relative flux during HA filtration. Each curve represents an average of 4 samples.

Fouling of TiO₂ nanocomposite membranes was less severe than that of ZnO-nanocomposite membranes. The improved anti-fouling properties of TiO₂ nanocomposite membranes could be due to a decrease in surface porosity hence decreasing surface roughness compared to ZnO-nanocomposite membranes (96). It could also be due to a decrease in permeation drag, where pure water flux recorded for ZnO-nanocomposite membranes was twice as high as that of TiO₂ nanocomposite membranes (54). It could also be due to a lower affinity of TiO₂ nanocomposite membranes to interact with HA compared to ZnO-nanocomposite membranes.

In order to determine the affinity of TiO₂ nanocomposite membranes towards HA, static adsorption test was carried out. The percentage of weight increase after static adsorption is shown in Figure 36. Weight percentage recorded decreases as TiO₂ concentration increases. Indicating an improved hydrophilicity of membranes and reduced affinity towards HA and a reduced affinity of TiO₂ nanocomposite membranes to interact with HA.

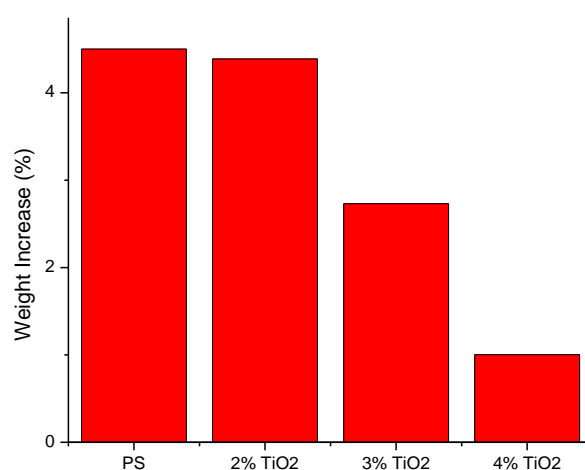


Figure 37 effect of TiO₂ in the membrane on the percentage of weight increase during static adsorption test.

The rejection of HA during the fouling experiments is shown in Figure 38. There seems to be a slight increase in rejection for TiO₂-nanocomposite membranes compared to the PS membranes. This is mainly due to the decrease in mean pore diameter (Table 4).

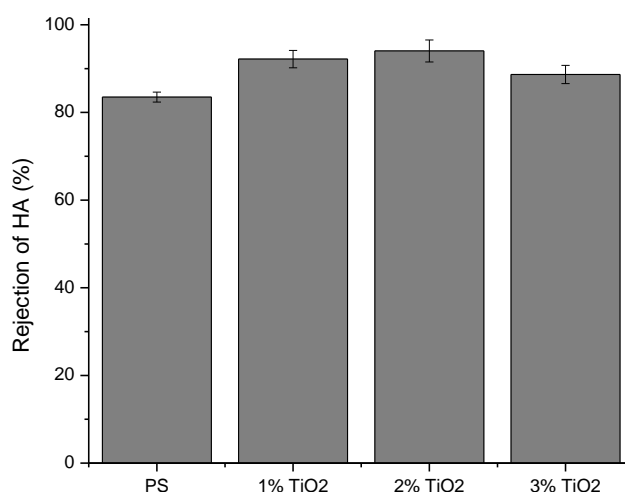


Figure 38. Effect of TiO₂ concentration on HA rejection. Each bar represents the average of 4 samples.

TiO₂-nanocomposite membranes were tested for cleanability using fouling recovery ratio (FRR). The FRR of TiO₂-nanocomposite membranes did not show a significant improvement compared to 0% membranes. This could be due to an increase in porosity of TiO₂-nanocomposite membranes, which makes it harder to remove HA from the membrane surface “valleys”. However, compared to ZnO-nanocomposite membranes, an improvement in FRR was noted for TiO₂-nanocomposite membranes. Which indicated a lower affinity of TiO₂-nanocomposite membranes to interact with HA as shown in Figure 39. Where the TiO₂-nanocomposite membranes showed similar discoloration as the polysulfone membranes.

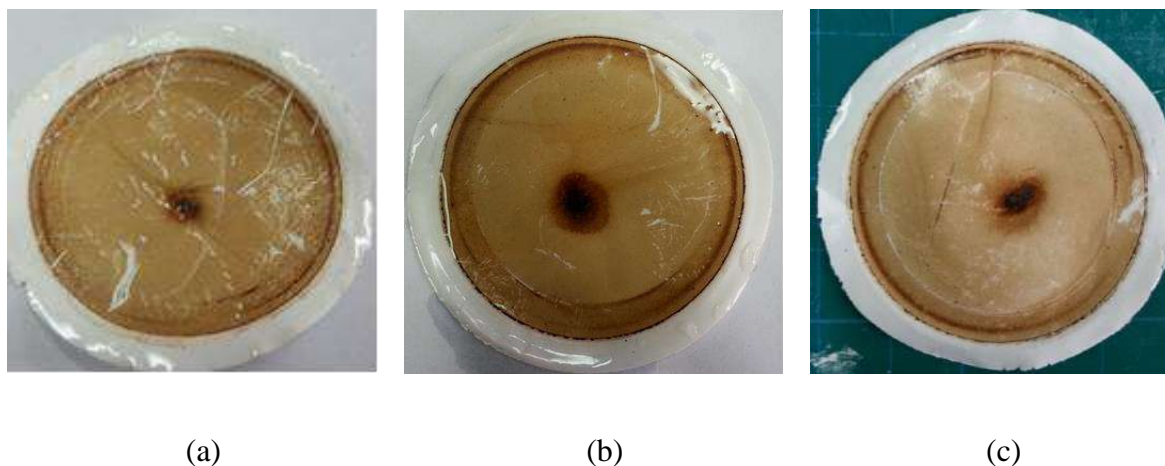


Figure 39 Appearance of different membranes after HA fouling experiments a) PS, b) 1% TiO₂ nanocomposite membranes, c) 4% TiO₂ nanocomposite membranes

5.2 Conclusions

The fabricated TiO₂-nanocomposite membranes exhibited an improved water flux compared to PS membranes. However, there was no significant change in pure water flux as the concentration of TiO₂ NP's increases. TiO₂-nanocomposite membranes had a lower water flux than ZnO-nanocomposite membranes. The difference in flux between TiO₂ and ZnO-nanocomposite membranes was attributed to the decrease in TiO₂-nanocomposite membranes surface porosity compared to the surface porosity of ZnO-nanocomposite membranes.

The decrease in porosity of TiO₂-nanocomposite membranes compared to ZnO-nanocomposite membranes was attributed to the increase in TiO₂-PS casting solution viscosity. Where the water movement into the TiO₂-PS polymer film is hindered. On the other hand, the presence of ZnO NP's in the casting seem to propel water molecules movement into the polymer film. The increase in viscosity of TiO₂-PS casting solution suppressed macrovoids formation. The suppression of macrovoids reduced TiO₂-nanocomposite membranes sensitivity to pressure application i.e. compaction.

TiO₂-nanocomposite membranes showed an improved anti-fouling properties compared to PS and ZnO-nanocomposite membranes. Indicating an increase in hydrophilicity of TiO₂-nanocomposite membranes surface and a decreased affinity to interact with HA. FRR of TiO₂-nanocomposite membranes did not improved compared to PS membranes. This was attributed to the increase in TiO₂-nanocomposite membranes porosity i.e. roughness, which causes HA to accumulate on the membranes surface and be harder to remove.

Chapter 6: Summary and Future Work

In today's world, it is important to develop a method where clean water can be obtained in large quantities and at a low price. Reclamation of polluted water or of surface water is hampered by fouling. Fouling is the main challenge facing membranes based operations. Nanocomposite membranes could become a possible solution for fouling. By reducing membranes interaction with foulants. The addition of nano-sized additives to membranes could possibly enhance membranes mechanical strength, and improve water permeation.

Two nano-fillers have been investigated in this work, zinc oxide (ZnO) and titanium dioxide (TiO₂). ZnO and TiO₂ were chosen because of their reported hydrophilic nature, hence reducing membranes surface hydrophobicity and reducing the interaction between foulants and membrane surface. Other advantages ZnO and TiO₂ include their wide commercial applications, their high toxicity threshold as well as their relatively low price. The following sections summarizes the work that has been done in this thesis

6.1 Fabrication and performance of ZnO-nanocomposite membranes: A summary

Fabrication of ZnO-nanocomposite membranes was carried out using wet phase inversion.

The fabrication procedure was relatively simple. ZnO NP's were not coated or modified in any way. ZnO-nanocomposite were tested for their performance in four steps. First membranes were operated at higher pressure (5 bar) than that used for the rest of the tests. This was done to study the initial flux decay caused by the deformation of membranes internal structure. The second step was to test membranes for pure water flux and use it as a baseline. The third experiment aimed at testing membranes flux decay during humic acid (HA) filtration. The final step was to determine membrane cleanability by filtrating pure water (without stirring) and calculating the flux recovery ratio.

ZnO-nanocomposite membranes had an excellent increase in pure water flux. The increase in pure water flux was found to be a function of ZnO NP's loading with the highest pure water flux being for 4% membranes. The internal structure of membranes was found to have an increased number of macrovoids, which contributed to the initial decay in flux. Membranes surface porosity was also a function of ZnO loading, with increasing ZnO loading an increase in porosity was observed.

The fouling of ZnO-nanocomposite membranes was aggravated compared to 0% PS membranes. The large decrease in flux and the formation of a compact dense layer of foulants on top of the membranes surface was attributed to two parameters: The higher permeation drag caused by higher initial flux (physical aspect) and the release of Zn^{+2} from membranes surface as well as the adoption of HA on ZnO NP's surface. The fouling recovery ratio of ZnO-nanocomposite membranes was lower than 0% membranes. Indicating a strong adsorption of HA on the membrane surface.

In the end, it was concluded that the combined effect of aggravated fouling by HA and the release of Zn^{+2} from ZnO-nanocomposite membranes makes ZnO NP's an unsuitable nano-filler for membranes modification. A better choice would be another hydrophilic nanoparticles with commercial availability and chemical and thermal stability. The choice was made to use TiO_2 NP's to fabricate TiO_2 -nanocomposite membranes. The following section summarizes the results obtained for TiO_2 -nanocomposite membranes.

6.2 Fabrication and performance of TiO_2 -nanocomposite membranes: A summary

On the other hand, TiO_2 -nanocomposite membranes had an improved anti-fouling compared to both PS and ZnO-nanocomposite membranes. It seems that TiO_2 NP's increased the hydrophilicity of TiO_2 -nanocomposite membranes surface. TiO_2 -nanocomposite membranes performance was almost the same even at higher TiO_2 NP's loading. This could be due to inefficient dispersion of TiO_2 NP's prior to casting.

It is finally concluded that nanocomposite membranes performance is dictated by the filler interaction with foulants. Nanocomposite membranes surface and internal structure are affected by the interaction of nano-filler and polymer. If the nano-filler and polymer have a higher interaction (TiO_2 -PS), would have a fewer macrovoids and be less sensitive to the application of pressure.

6.3 Recommendations for future work

This work has raised the following question, what is the extent of nano-fillers dominance on the interaction of foulants with membranes surface? It is obvious that ZnO and TiO_2 had different behavior due to their respective different properties. Thus, it is safe to assume that nano-fillers will govern the behavior of nanocomposite membranes. This

study is considered the first step in understanding natural organic matter (NOM) interaction with nanocomposite membranes. There are several topics on which a future studies could be based:

- 1- Investigate the cleanability of nanocomposite membranes using chemical cleaning methods such as NaOH and EDTA. This is done in order to investigate the strength of the interaction between nanocomposite membranes and foulants.
- 2- Modification of nanoparticles surface using a hydrophilic monomer such as acrylic acid or 2-Hydroxyethyl methacrylate (HEMA). Modification could be achieved using radical initiation.
- 3- Study other potential nano-fillers, such as Aluminum oxide and copper oxide.
- 4- Study the environmental impact of nanocomposite membranes, whether or not nanoparticles are released to the environment. This is especially relevant, since ZnO-nanocomposite membranes were found to release (Zn^{+2}), which is a toxic for aquatic life and was found to be cytotoxic for mammalian cells.

References

1. Water Scarcity | Threats | WWF (Internet). World Wildlife Fund. (cited 2015 Jul 15). Available from: <https://www.worldwildlife.org/threats/water-scarcity>
2. Jordan - Geography and Environment - Jordan's Water Shortage (Internet). (cited 2015 Jul 15). Available from: http://www.kinghussein.gov.jo/geo_env4.html
3. Water Authority of Jordan - Web Presence (Internet). (cited 2015 Jan 1). Available from: <http://www.waj.gov.jo/sites/en-us/default.aspx>
4. Baker R. Membrane Technology and Applications. 2nd ed. Jhon Wiley & Sons; 2004.
5. Nunes SP, Peinemann K-V. Membrane Technology: in the Chemical Industry. 1st ed. Wiley-VCH; 2001.
6. Matsuura T. Synthetic Membranes and Membrane Separation Processes. CRC Press; 1993. 482 p.
7. Soren P. Beier. Pressure Driven Membrane Processes.
8. Cussler EL. Diffusion: Mass Transfer in Fluid Systems. Cambridge University Press; 1997. 606 p.
9. Pinnau I., Freeman B. D. Formation and Modification of Polymeric Membranes: Overview. Membrane Formation and Modification (Internet). American Chemical Society; 1999 (cited 2014 Mar 1). p. 1–22. Available from: <http://dx.doi.org/10.1021/bk-2000-0744.ch001>
10. Lalia BS, Kochkodan V, Hashaikeh R, Hilal N. A review on membrane fabrication: Structure, properties and performance relationship. Desalination. 2013 Oct 1;326:77–95.
11. Loeb S. The Loeb-Sourirajan Membrane: How It Came About. Synthetic Membranes. Chapter 1: American Chemical Society; 1981.
12. Lee K-W, Seo B-K, Nam S-T, Han M-J. Trade-off between thermodynamic enhancement and kinetic hindrance during phase inversion in the preparation of polysulfone membranes. Desalination. 2003 Nov 5;159(3):289–96.

13. Molina S, Carretero P, Teli SB, la Campa JG de, Lozano ÁE, de Abajo J. Hydrophilic porous asymmetric ultrafiltration membranes of aramid-g-PEO copolymers. *J Membr Sci.* 2014 Mar 15;454:233–42.
14. Nair AK, Isloor AM, Kumar R, Ismail AF. Antifouling and performance enhancement of polysulfone ultrafiltration membranes using CaCO₃ nanoparticles. *Desalination.* 2013 Aug 1;322:69–75.
15. Möckel D, Staude E, Guiver MD. Static protein adsorption, ultrafiltration behavior and cleanability of hydrophilized polysulfone membranes. *J Membr Sci.* 1999 Jun 1;158(1–2):63–75.
16. Zhao S, Wang Z, Wei X, Zhao B, Wang J, Yang S, et al. Performance improvement of polysulfone ultrafiltration membrane using PANiEB as both pore forming agent and hydrophilic modifier. *J Membr Sci.* 2011 Dec 1;385–386:251–62.
17. Song Zhao, Zhi Wang, Wei X, Zhao B, Wang J, Yang S, et al. Performance Improvement of Polysulfone Ultrafiltration Membrane Using Well-Dispersed Polyaniline–Poly(vinylpyrrolidone) Nanocomposite as the Additive. *Ind Eng Chem Res.* 2012 Mar 28;51(12):4661–72.
18. Zhao C, Xue J, Ran F, Sun S. Modification of polyethersulfone membranes – A review of methods. *Prog Mater Sci.* 2013 Jan;58(1):76–150.
19. Cao X, Ma J, Shi X, Ren Z. Effect of TiO₂ nanoparticle size on the performance of PVDF membrane. *Appl Surf Sci.* 2006 Dec 15;253(4):2003–10.
20. Lalia BS, Kochkodan V, Hashaikeh R, Hilal N. A review on membrane fabrication: Structure, properties and performance relationship. *Desalination.* 2013 Oct 1;326:77–95.
21. van de Witte P, Dijkstra PJ, van den Berg JWA, Feijen J. Phase separation processes in polymer solutions in relation to membrane formation. *J Membr Sci.* 1996 Aug 21;117(1–2):1–31.
22. Barth C, Gonçalves MC, Pires ATN, Roeder J, Wolf BA. Asymmetric polysulfone and polyethersulfone membranes: effects of thermodynamic conditions during formation on their performance. *J Membr Sci.* 2000 May 1;169(2):287–99.

23. Barton BF, Reeve JL, McHugh AJ. Observations on the dynamics of nonsolvent-induced phase inversion. *J Polym Sci Part B Polym Phys*. 1997;35(4):569–85.
24. Leo CP, Cathie Lee WP, Ahmad AL, Mohammad AW. Polysulfone membranes blended with ZnO nanoparticles for reducing fouling by oleic acid. *Sep Purif Technol*. 2012 Mar 22;89:51–6.
25. Alsari AM. The effect of sodium dodecyl sulfate solutions as gelation media on the formation of PES membranes. (Internet). University of Ottawa (Canada).; 2000 (cited 2015 Jan 26). Available from: <http://www.ruor.uottawa.ca/handle/10393/8670>
26. Crock CA, Rogensues AR, Shan W, Tarabara VV. Polymer nanocomposites with graphene-based hierarchical fillers as materials for multifunctional water treatment membranes. *Water Res*. 2013 Aug 1;47(12):3984–96.
27. Tweddle TA, Striez C, Tam CM, Hazlett JD. Polysulfone membranes I. performance comparison of commercially available ultrafiltration membranes. *Desalination*. 1992 Apr;86(1):27–41.
28. Strathmann H, Scheible P, Baker RW. A rationale for the preparation of Loeb-Sourirajan-type cellulose acetate membranes. *J Appl Polym Sci*. 1971;15(4):811–28.
29. Ahmad AL, Ooi BS, Wahab Mohammad A, Choudhury JP. Development of a highly hydrophilic nanofiltration membrane for desalination and water treatment. *Desalination*. 2004 Aug 15;168:215–21.
30. Lau WJ, Ismail AF, Misdan N, Kassim MA. A recent progress in thin film composite membrane: A review. *Desalination*. 2012 Feb 15;287:190–9.
31. Veríssimo S, Peinemann K-V, Bordado J. Influence of the diamine structure on the nanofiltration performance, surface morphology and surface charge of the composite polyamide membranes. *J Membr Sci*. 2006 Aug 1;279(1–2):266–75.
32. Tang CY, Kwon Y-N, Leckie JO. Probing the nano- and micro-scales of reverse osmosis membranes—A comprehensive characterization of physiochemical properties of uncoated and coated membranes by XPS, TEM, ATR-FTIR, and streaming potential measurements. *J Membr Sci*. 2007 Jan 5;287(1):146–56.

33. Beasley JK. The evaluation and selection of polymeric materials for reverse osmosis membranes. *Desalination*. 1977 Dec;22(1–3):181–9.
34. Bernstein R, Belfer S, Freger V. Toward Improved Boron Removal in RO by Membrane Modification: Feasibility and Challenges. *Env Sci Technol*. 2011;45(8):3613–20.
35. Belfer S, Fainshtain R, Purinson Y, Gilron J, Nyström M, Mänttari M. Modification of NF membrane properties by in situ redox initiated graft polymerization with hydrophilic monomers. *J Membr Sci*. 2004 Aug 1;239(1):55–64.
36. Abuhabib AA, Mohammad AW, Hilal N, Rahman RA, Shafie AH. Nanofiltration membrane modification by UV grafting for salt rejection and fouling resistance improvement for brackish water desalination. *Desalination*. 2012 Jun 1;295:16–25.
37. Choi J-S, Hwang T-M, Lee S, Hong S. A systematic approach to determine the fouling index for a RO/NF membrane process. *Desalination*. 2009 Mar;238(1–3):117–27.
38. Zazouli MA, Nasseri S, Ulbricht M. Fouling effects of humic and alginic acids in nanofiltration and influence of solution composition. *Desalination*. 2010 Jan 15;250(2):688–92.
39. Elimelech M, Phillip WA. The Future of Seawater Desalination: Energy, Technology, and the Environment. *Science*. 2011 Aug 5;333(6043):712–7.
40. Tang CY, Leckie JO. Membrane Independent Limiting Flux for RO and NF Membranes Fouled by Humic Acid. *Env Sci Technol*. 2007;41(13):4767–73.
41. Mosqueda-Jimenez D, Narbaitz R, Matsuura T. Membrane Fouling Test: Apparatus Evaluation. *J Environ Eng*. 2004;130(1):90–9.
42. Cui ZF, Muralidhara HS. *Membrane Technology: A Practical Guide to Membrane Technology and Applications in Food and Bioprocessing*. Elsevier; 2010. 307 p.
43. Jarusutthirak C, Amy G, Croué J-P. Fouling characteristics of wastewater effluent organic matter (EfOM) isolates on NF and UF membranes. *Desalination*. 2002 Sep 10;145(1–3):247–55.

44. Zularisam AW, Ismail AF, Salim MR, Sakinah M, Hiroaki O. Fabrication, fouling and foulant analyses of asymmetric polysulfone (PSF) ultrafiltration membrane fouled with natural organic matter (NOM) source waters. *J Membr Sci.* 2007 Aug 1;299(1–2):97–113.
45. Wang R, Dong W, Ruan C, Kanayeva D, Tian R, Lassiter K, et al. TiO₂ nanowire bundle microelectrode based impedance immunosensor for rapid and sensitive detection of *Listeria monocytogenes*. *Nano Lett.* 2008 Sep;8(9):2625–31.
46. Wang F, Tarabara VV. Pore blocking mechanisms during early stages of membrane fouling by colloids. *J Colloid Interface Sci.* 2008 Dec 15;328(2):464–9.
47. Koseoglu-Imer DY, Kose B, Altinbas M, Koyuncu I. The production of polysulfone (PS) membrane with silver nanoparticles (AgNP): Physical properties, filtration performances, and biofouling resistances of membranes. *J Membr Sci.* 2013 Feb 1;428:620–8.
48. Ben-Sasson M, Zodrow KR, Genggeng Q, Kang Y, Giannelis EP, Elimelech M. Surface Functionalization of Thin-Film Composite Membranes with Copper Nanoparticles for Antimicrobial Surface Properties. *Environ Sci Technol.* 2014 Jan 7;48(1):384–93.
49. Seidel A, Elimelech M. Coupling between chemical and physical interactions in natural organic matter (NOM) fouling of nanofiltration membranes: implications for fouling control. *J Membr Sci.* 2002 Jun 30;203(1–2):245–55.
50. Elimelech M, Bhattacharjee S. A novel approach for modeling concentration polarization in crossflow membrane filtration based on the equivalence of osmotic pressure model and filtration theory. *J Membr Sci.* 1998 Jul 8;145(2):223–41.
51. Srisurichan S, Jiraratananon R, Fane AG. Humic acid fouling in the membrane distillation process. *Desalination.* 2005 Apr 1;174(1):63–72.
52. Mänttäre M, Puro L, Nuortila-Jokinen J, Nyström M. Fouling effects of polysaccharides and humic acid in nanofiltration. *J Membr Sci.* 2000 Jan 17;165(1):1–17.
53. Tang CY, Kwon Y-N, Leckie JO. Characterization of Humic Acid Fouled Reverse Osmosis and Nanofiltration Membranes by Transmission Electron Microscopy and Streaming Potential Measurements. *Env Sci Technol.* 2006;41(3):942–9.

54. Hong S, Elimelech M. Chemical and physical aspects of natural organic matter (NOM) fouling of nanofiltration membranes. *J Membr Sci.* 1997 Sep 3;132(2):159–81.
55. Amoudi A Al-, Lovitt RW. Fouling strategies and the cleaning system of NF membranes and factors affecting cleaning efficiency. *J Membr Sci.* 2007 Oct 15;303(1–2):4–28.
56. Mänttari M, Puro L, Nuortila-Jokinen J, Nyström M. Fouling effects of polysaccharides and humic acid in nanofiltration. *J Membr Sci.* 2000 Jan 17;165(1):1–17.
57. Song L, Elimelech M. Theory of concentration polarization in crossflow filtration. *J Chem Soc Faraday Trans.* 1995 Jan 1;91(19):3389–98.
58. Tang CY, Kwon Y-N, Leckie JO. Fouling of reverse osmosis and nanofiltration membranes by humic acid—Effects of solution composition and hydrodynamic conditions. *J Membr Sci.* 2007 Mar 1;290(1–2):86–94.
59. Abu Seman MN, Khayet M, Hilal N. Development of antifouling properties and performance of nanofiltration membranes modified by interfacial polymerisation. *Desalination.* 2011 Jun 1;273(1):36–47.
60. Kang G, Cao Y. Development of antifouling reverse osmosis membranes for water treatment: A review. *Water Res.* 2012 Mar 1;46(3):584–600.
61. Khulbe KC, Feng C, Matsuura T. The art of surface modification of synthetic polymeric membranes. *J Appl Polym Sci.* 2010;115(2):855–95.
62. Romero-Vargas Castrillón S, Lu X, Shaffer DL, Elimelech M. Amine enrichment and poly(ethylene glycol) (PEG) surface modification of thin-film composite forward osmosis membranes for organic fouling control. *J Membr Sci.* 2014 Jan 15;450:331–9.
63. Bernstein R, Belfer S, Freger V. Surface Modification of Dense Membranes Using Radical Graft Polymerization Enhanced by Monomer Filtration. *Langmuir.* 2010 Jul 20;26(14):12358–65.
64. Malaisamy R, Bruening ML. High-Flux Nanofiltration Membranes Prepared by Adsorption of Multilayer Polyelectrolyte Membranes on Polymeric Supports.

Langmuir. 2005 Nov 1;21(23):10587–92.

65. Nasef MM, Güven O. Radiation-grafted copolymers for separation and purification purposes: Status, challenges and future directions. *Prog Polym Sci.* 2012 Dec;37(12):1597–656.
66. Lau WWY, Jiang Y. Performance of polysulfone/carboxylated polysulfone membranes. *Polym Int.* 1994;33(4):413–7.
67. Sajitha CJ, Mahendran R, Mohan D. Studies on cellulose acetate–carboxylated polysulfone blend ultrafiltration membranes—Part I. *Eur Polym J.* 2002 Dec;38(12):2507–11.
68. Park JY, Acar MH, Akthakul A, Kuhlman W, Mayes AM. Polysulfone-graft-poly(ethylene glycol) graft copolymers for surface modification of polysulfone membranes. *Biomaterials.* 2006 Feb;27(6):856–65.
69. Zhao S, Wang Z, Wei X, Zhao B, Wang J, Yang S, et al. Performance Improvement of Polysulfone Ultrafiltration Membrane Using Well-Dispersed Polyaniline–Poly(vinylpyrrolidone) Nanocomposite as the Additive. *Ind Eng Chem Res.* 2012 Mar 28;51(12):4661–72.
70. Radovanovic P, Thiel SW, Hwang S-T. Formation of asymmetric polysulfone membranes by immersion precipitation. Part II. The effects of casting solution and gelation bath compositions on membrane structure and skin formation. *J Membr Sci.* 1992 Jan 15;65(3):231–46.
71. Mauter MS, Wang Y, Okemgbo KC, Osuji CO, Giannelis EP, Elimelech M. Antifouling Ultrafiltration Membranes via Post-Fabrication Grafting of Biocidal Nanomaterials. *ACS Appl Mater Interfaces.* 2011 Aug 24;3(8):2861–8.
72. Teli SB, Molina S, Sotto A, Calvo EG, Abajob J de. Fouling Resistant Polysulfone–PANI/TiO₂ Ultrafiltration Nanocomposite Membranes. *Ind Eng Chem Res.* 2013 Jul 10;52(27):9470–9.
73. Nanoscience and Nanotechnologies: Opportunities and Uncertainties. Royal Society; 2004. 116 p.
74. Zhang G, Lu S, Zhang L, Meng Q, Shen C, Zhang J. Novel polysulfone hybrid ultrafiltration membrane prepared with TiO₂-g-HEMA and its antifouling

characteristics. *J Membr Sci.* 2013 Jun 1;436:163–73.

75. The Royal Society & The Royal Academy of Engineering. Nanoscience and nanotechnologies: opportunities and uncertainties (Internet). The Royal Society, London; 2004 (cited 2014 May 17). Available from: <http://www.nanotec.org.uk/finalReport.htm>
76. Eita M, Wågberg L, Muhammed M. Thin Films of Zinc Oxide Nanoparticles and Poly(acrylic acid) Fabricated by the Layer-by-Layer Technique: a Facile Platform for Outstanding Properties. *J Phys Chem C.* 2012 Feb 23;116(7):4621–7.
77. de Lannoy C-F, Soyer E, Wiesner MR. Optimizing carbon nanotube-reinforced polysulfone ultrafiltration membranes through carboxylic acid functionalization. *J Membr Sci.* 2013 Nov 15;447:395–402.
78. Mierzwa JC, Arieta V, Verlage M, Carvalho J, Vecitis CD. Effect of clay nanoparticles on the structure and performance of polyethersulfone ultrafiltration membranes. *Desalination.* 2013 Apr 2;314:147–58.
79. Phelane L, Muya FN, Richards HL, Baker PGL, Iwuoha EI. Polysulfone Nanocomposite Membranes with improved hydrophilicity. *Electrochimica Acta.* 2014 May 10;128:326–35.
80. Ng LY, Mohammad AW, Leo CP, Hilal N. Polymeric membranes incorporated with metal/metal oxide nanoparticles: A comprehensive review. *Desalination.* 2013 Jan 2;308:15–33.
81. Wang P, Ma J, Shi F, Ma Y, Wang Z, Zhao X. Behaviors and Effects of Differing Dimensional Nanomaterials in Water Filtration Membranes through the Classical Phase Inversion Process: A Review. *Ind Eng Chem Res.* 2013 Aug 7;52(31):10355–63.
82. Yang Y, Zhang H, Wang P, Zheng Q, Li J. The influence of nano-sized TiO₂ fillers on the morphologies and properties of PSF UF membrane. *J Membr Sci.* 2007 Feb 1;288(1–2):231–8.
83. Bae T-H, Tak T-M. Effect of TiO₂ nanoparticles on fouling mitigation of ultrafiltration membranes for activated sludge filtration. *J Membr Sci.* 2005 Mar 1;249(1–2):1–8.

84. Hamid NAA, Ismail AF, Matsuura T, Zularisam AW, Lau WJ, Yuliwati E, et al. Morphological and separation performance study of polysulfone/titanium dioxide (PSF/TiO₂) ultrafiltration membranes for humic acid removal. *Desalination*. 2011 Jun 1;273(1):85–92.
85. Zhang G, Lu S, Zhang L, Meng Q, Shen C, Zhang J. Novel polysulfone hybrid ultrafiltration membrane prepared with TiO₂-g-HEMA and its antifouling characteristics. *J Membr Sci*. 2013 Jun 1;436:163–73.
86. Balta S, Sotto A, Luis P, Benea L, Van der Bruggen B, Kim J. A new outlook on membrane enhancement with nanoparticles: The alternative of ZnO. *J Membr Sci*. 2012 Feb 1;389:155–61.
87. Hong J, He Y. Effects of nano sized zinc oxide on the performance of PVDF microfiltration membranes. *Desalination*. 2012 Sep 17;302:71–9.
88. Franklin NM, Rogers NJ, Apte SC, Batley GE, Gadd GE, Casey PS. Comparative Toxicity of Nanoparticulate ZnO, Bulk ZnO, and ZnCl₂ to a Freshwater Microalga (*Pseudokirchneriella subcapitata*): The Importance of Particle Solubility. *Environ Sci Technol*. 2007 Dec 1;41(24):8484–90.
89. Bondarenko O, Juganson K, Ivask A, Kasemets K, Mortimer M, Kahru A. Toxicity of Ag, CuO and ZnO nanoparticles to selected environmentally relevant test organisms and mammalian cells in vitro: a critical review. *Arch Toxicol*. 2013 Jul;87(7):1181–200.
90. Rahimpour A, Madaeni SS, Mansourpanah Y. Nano-porous polyethersulfone (PES) membranes modified by acrylic acid (AA) and 2-hydroxyethylmethacrylate (HEMA) as additives in the gelation media. *J Membr Sci*. 2010 Nov 15;364(1–2):380–8.
91. Singh S, Khulbe KC, Matsuura T, Ramamurthy P. Membrane characterization by solute transport and atomic force microscopy. *J Membr Sci*. 1998 Feb 2;142(1):111–27.
92. Khayet M, Matsuura T. Application of surface modifying macromolecules for the preparation of membranes for membrane distillation. *Desalination*. 2003 Aug 1;158(1-3):51–6.
93. Xie Y, He Y, Irwin PL, Jin T, Shi X. Antibacterial Activity and Mechanism of Action of Zinc Oxide Nanoparticles against *Campylobacter jejuni*. *Appl Environ*

Microbiol. 2011 Apr;77(7):2325–31.

94. Baker R. Membrane Technology and Applications. 2nd ed. Wiley; 2004.
95. McCutcheon JR, Elimelech M. Influence of membrane support layer hydrophobicity on water flux in osmotically driven membrane processes. *J Membr Sci.* 2008 Jun 20;318(1–2):458–66.
96. Alsari AM, Khulbe KC, Matsuura T. The effect of sodium dodecyl sulfate solutions as gelation media on the formation of PES membranes. *J Membr Sci.* 2001 Jul 15;188(2):279–93.
97. Elimelech M, Zhu X, Childress AE, Hong S. Role of membrane surface morphology in colloidal fouling of cellulose acetate and composite aromatic polyamide reverse osmosis membranes. *J Membr Sci.* 1997 Apr 30;127(1):101–9.
98. Singh S, Khulbe K., Matsuura T, Ramamurthy P. Membrane characterization by solute transport and atomic force microscopy. *J Membr Sci.* 1998 Feb 2;142(1):111–27.
99. Rahimpour A, Jahanshahi M, Peyravi M, Khalili S. Interlaboratory studies of highly permeable thin-film composite polyamide nanofiltration membrane. *Polym Adv Technol.* 2012;23(5):884–93.
100. Smolders CA, Reuvers AJ, Boom RM, Wienk IM. Microstructures in phase-inversion membranes. Part 1. Formation of macrovoids. *J Membr Sci.* 1992 Oct 9;73(2–3):259–75.
101. Blanco J-F, Sublet J, Nguyen QT, Schaetzel P. Formation and morphology studies of different polysulfones-based membranes made by wet phase inversion process. *J Membr Sci.* 2006 Oct 20;283(1–2):27–37.
102. Radovanovic P, Thiel SW, Hwang S-T. Formation of asymmetric polysulfone membranes by immersion precipitation. Part I. Modelling mass transport during gelation. *J Membr Sci.* 1992 Jan 15;65(3):213–29.
103. Hussain YA, Saleh MH Al-. A viscoelastic-based model for TFC membranes flux reduction during compaction. *Desalination.* 2014 Jul 1;344:362–70.

104. Hussain YA, Saleh MH Al-, Ar-Ratrout SS. The effect of active layer non-uniformity on the flux and compaction of TFC membranes. *Desalination*. 2013 Nov 1;328:17–23.
105. Bohonak DM, Zydney AL. Compaction and permeability effects with virus filtration membranes. *J Membr Sci*. 2005 Jun 1;254(1–2):71–9.
106. Persson KM, Gekas V, Trägårdh G. Study of membrane compaction and its influence on ultrafiltration water permeability. *J Membr Sci*. 1995 Apr 14;100(2):155–62.
107. Yang K, Lin D, Xing B. Interactions of Humic Acid with Nanosized Inorganic Oxides. *Langmuir*. 2009 Mar 17;25(6):3571–6.
108. Yi Z, Zhu L-P, Xu Y-Y, Zhao Y-F, Ma X-T, Zhu B-K. Polysulfone-based amphiphilic polymer for hydrophilicity and fouling-resistant modification of polyethersulfone membranes. *J Membr Sci*. 2010 Dec 1;365(1–2):25–33.
109. Zhang G, Lu S, Zhang L, Meng Q, Shen C, Zhang J. Novel polysulfone hybrid ultrafiltration membrane prepared with TiO₂-g-HEMA and its antifouling characteristics. *J Membr Sci*. 2013 Jun 1;436:163–73.
110. Gerloff K, Fenoglio I, Carella E, Kolling J, Albrecht C, Boots AW, et al. Distinctive Toxicity of TiO₂ Rutile/Anatase Mixed Phase Nanoparticles on Caco-2 Cells. *Chem Res Toxicol*. 2012 Mar 19;25(3):646–55.
111. Auffan M, Rose J, Bottero J-Y, Lowry GV, Jolivet J-P, Wiesner MR. Towards a definition of inorganic nanoparticles from an environmental, health and safety perspective. *Nat Nanotechnol*. 2009 Oct;4(10):634–41.
112. Brinkert L, Abidine N, Aptel P. On the relation between compaction and mechanical properties for ultrafiltration hollow fibers. *J Membr Sci*. 1993 Feb 19;77(1):123–31.

Appendices

Appendix A: UV-Vis spectrum

UV-vis was used to determine the concentration of humic acid in permeate. A linear relationship was found between humic acid concentration and absorbance at λ 283 nm.

Figure 40 shows the linear relationship between humic acid and absorbance up to 50 ppm.

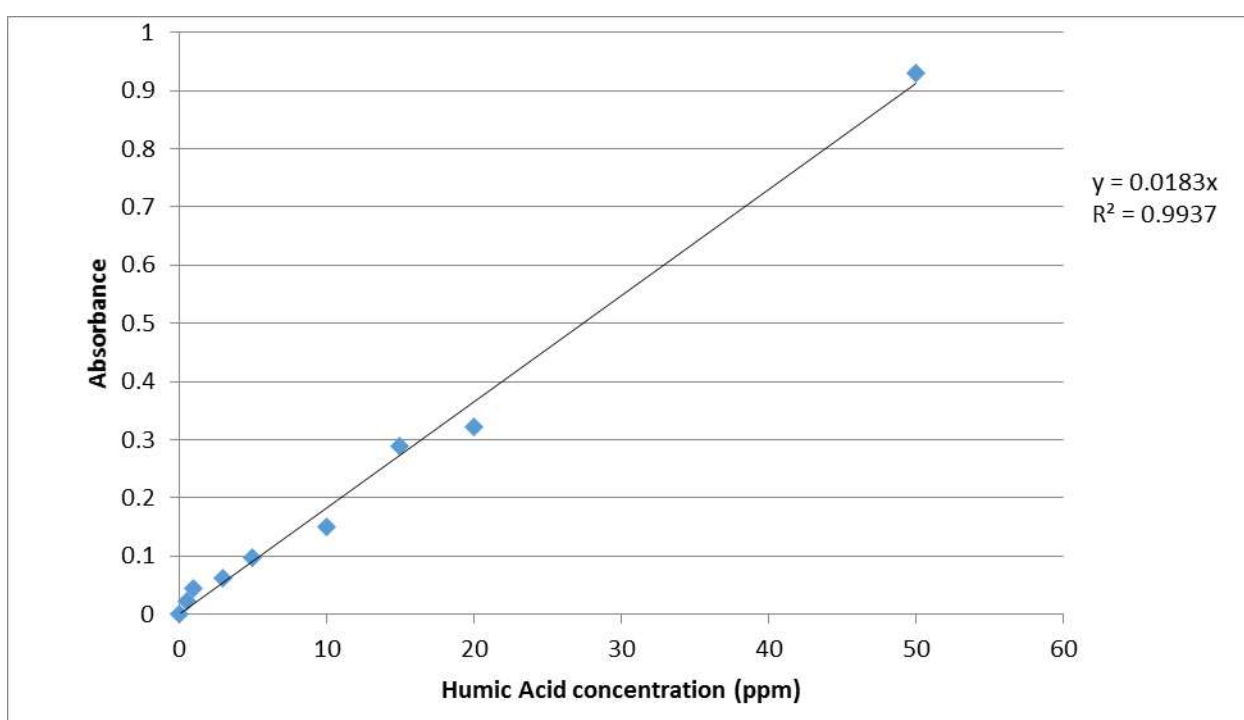


Figure 40 Concentration and absorbance of humic acid using UV-vis at λ 283 nm.

Appendix B: Pore size and pore size distribution graphical representation

The pore size and pore representation applied the MWCO data. The following graphs (Figure 41-Figure 45) represent the rejection data plotted against the logarithm of solute diameter.

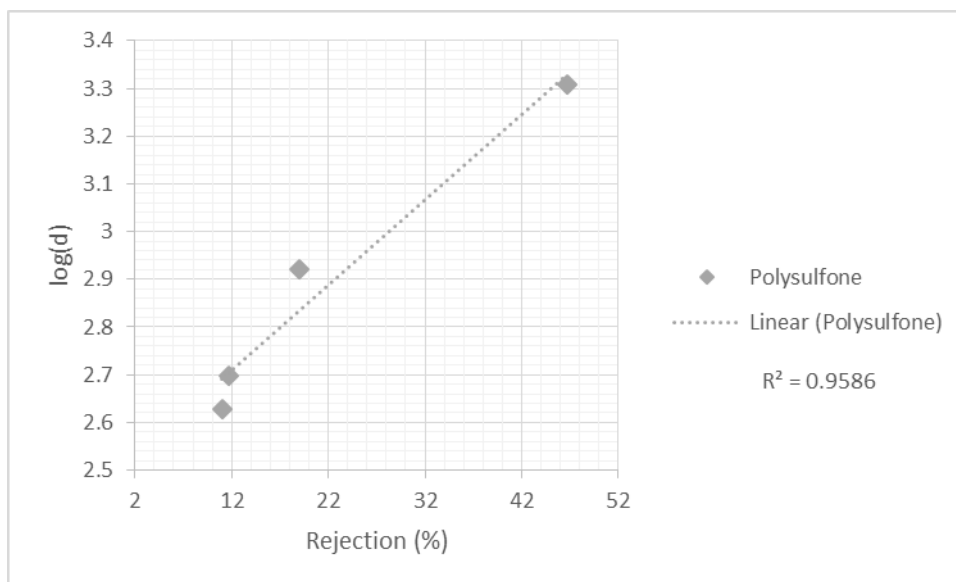


Figure 41 Solute separation curve of polysulfone. The rejection is plotted against $\log(d)$, where d is the diameter of PEG used in the solution

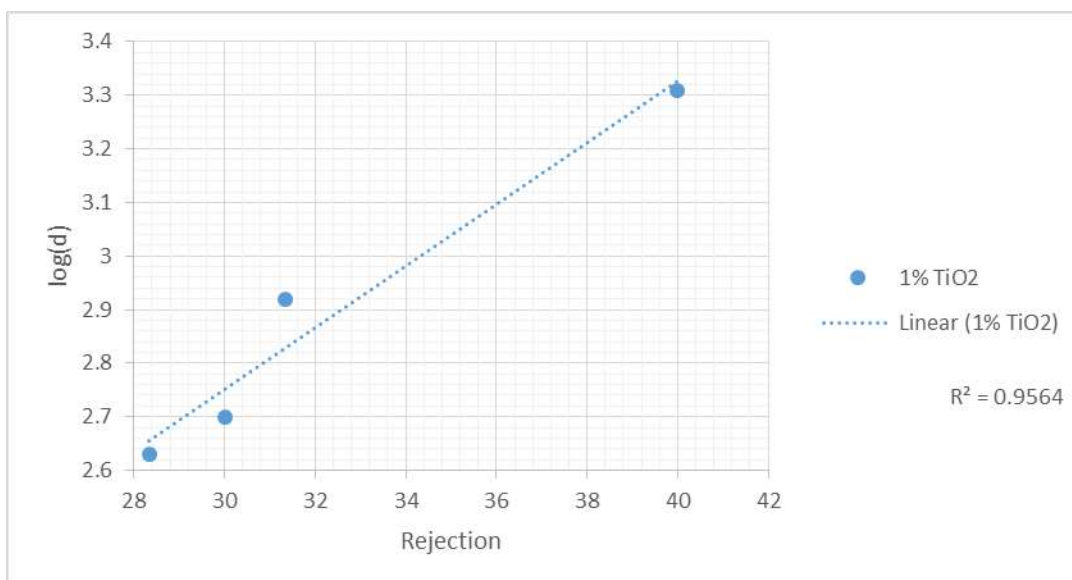


Figure 42 Solute separation curve of 1% TiO_2 . The rejection is plotted against $\log(d)$, where d is the diameter of PEG used in the solution.

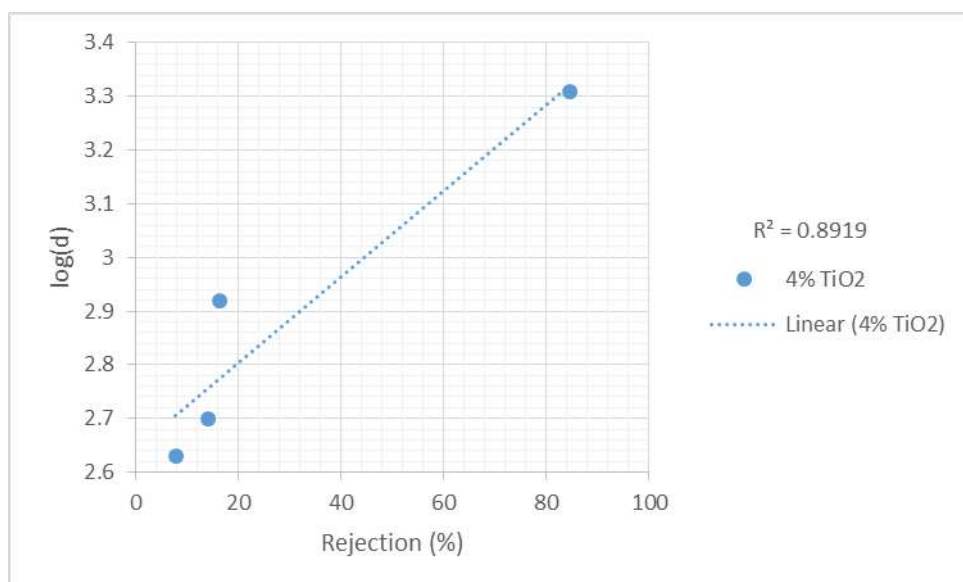


Figure 43 Solute separation curve of 4% TiO_2 . The rejection is plotted against $\log(d)$, where d is the diameter of PEG used in the solution.

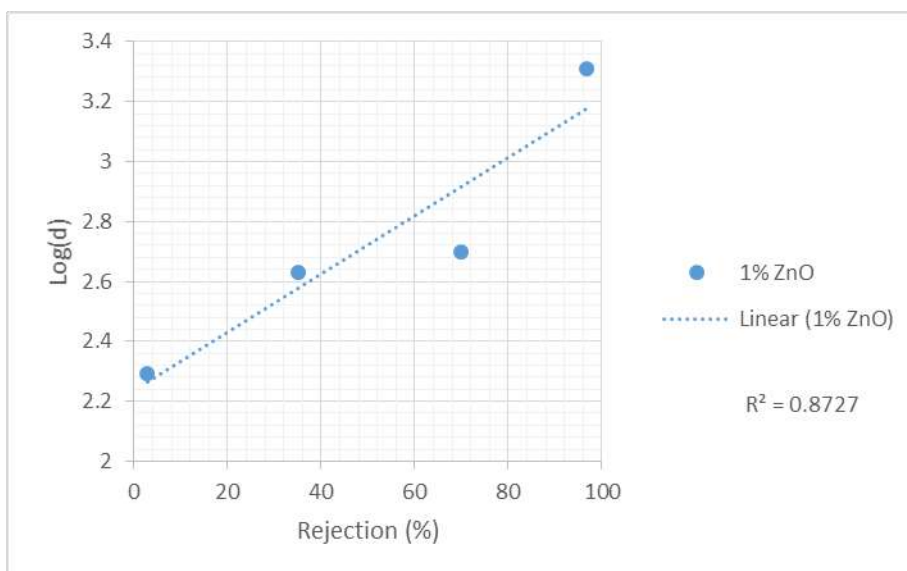


Figure 44 Solute separation curve of 1% ZnO. The rejection is plotted against $\log(d)$, where d is the diameter of PEG used in the solution.

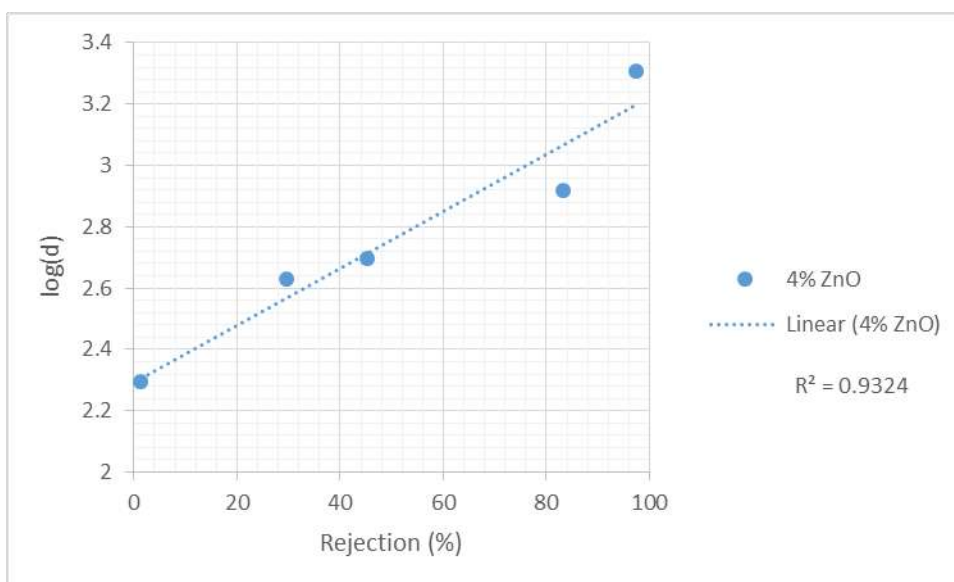


Figure 45 Solute separation curve of 4% ZnO. The rejection is plotted against $\log(d)$, where d is the diameter of PEG used in the solution

The pore distribution is presented in figures (Figure 46- Figure 48):

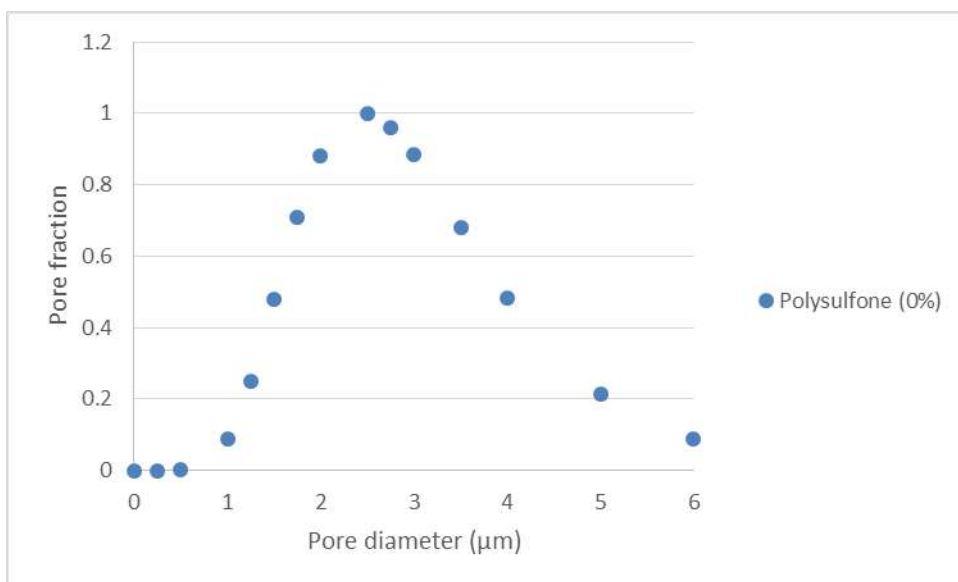


Figure 46 Pore size distribution of polysulfone (0%) membranes.

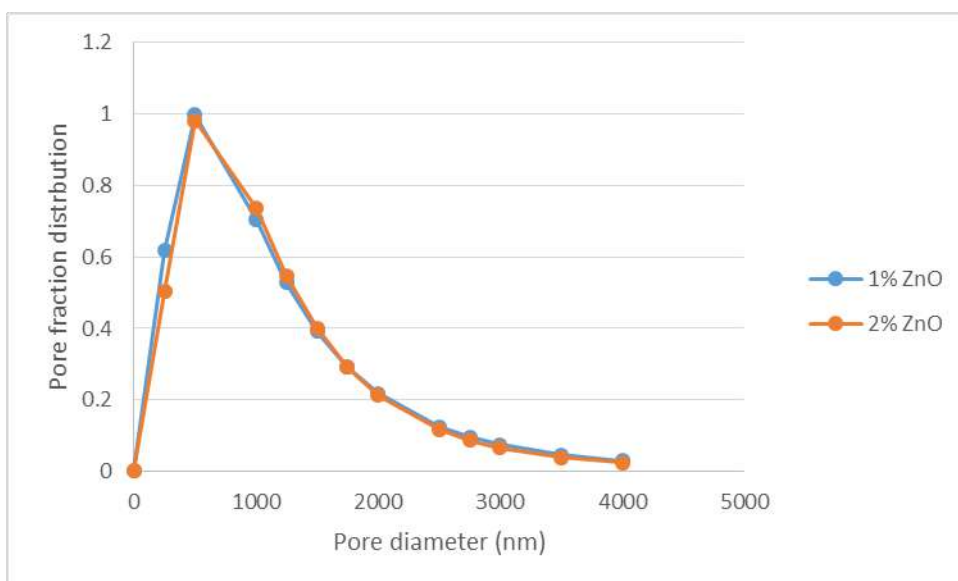


Figure 47 Pore distribution of 1% and 4% ZnO membranes.

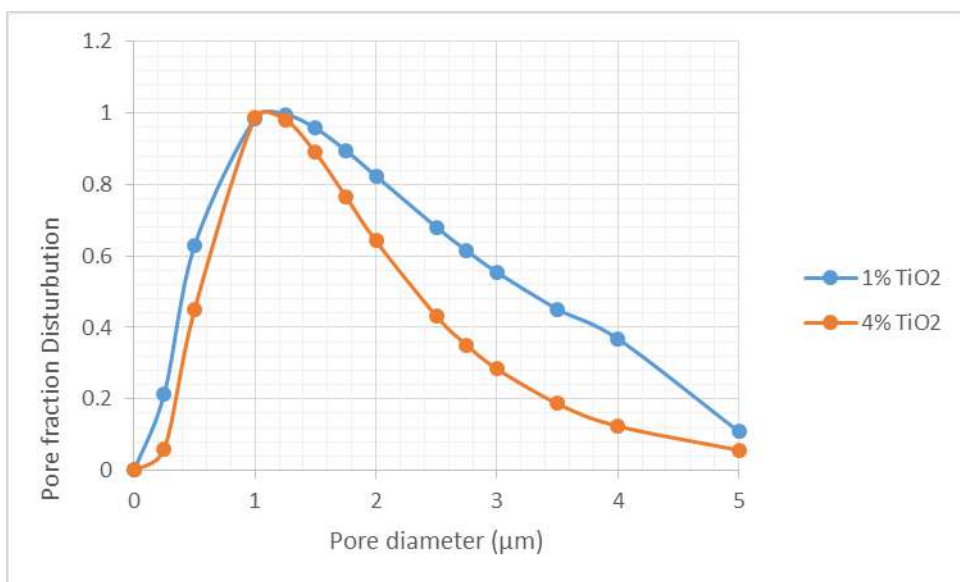


Figure 48 Pore distribution of 1% and 4% TiO₂ membranes

تصنيع أغشية ترشيح مقاومة للترسبات من مركبات نانوية البنية لأغراض معالجة المياه

إعداد: سكيانة سليمان الرطروط

الملخص

لقد أصبحت الأغشية البوليمرية المستخدمة في معالجة المياه جزءاً لا يتجزأ من محطات تنقية و معالجة المياه. و هذا بسبب المزايا العديدة التي تتحلّى بها هذه الأغشية، و لكن بالرغم من ذلك فإن الأغشية البوليمرية تعاني من عقبة تحول دون استخدامها بشكل دائم، ألا و هي الترسبات. هذا البحث يهدف إلى تصنيع أغشية بوليمرية فائقة النفاذية باستخدام مركبات نانوية البنية لتحسين بنية الأغشية البوليمرية و التقليل من حدوث الترسبات. لقد تمت دراسة دور المركبين "أكسيد الزنك" نانوي البنية و "ثاني أكسيد التيتانيوم" نانوي البنية في تفاعلها مع المواد العضوية الطبيعية و كيفية حدوث الترسبات باستخدام الأغشية المضاف لها مركبات نانوية البنية. لقد تم اختيار المركبين السابق ذكرهما لوجود عدد من الأبحاث التي تتعلق بطبيعتهما.

أظهرت نتائج دراسة الأغشية المصنعة بوجود مركب أكسيد الزنك نانوي البنية انجذاب هذه الأغشية نحو حمض الدبالية – أحد المواد العضوية الطبيعية- بالمقارنة مع الأغشية بولسلفونية البنية. هناك عدة أسباب تفسر انجذاب الأغشية المصنعة بوجود مركب أكسيد الزنك نانوي البنية، من الممكن أن يكون أحد الأسباب هو زيادة في نفاذية هذه الأغشية، مما يسبب زيادة في كمية الحمض المتواجد على سطح الغشاء و بالتالي زيادة في تكوين الترسبات. أحد الأسباب الأخرى قد تكون المساحة السطحية الكبيرة لأكسيد الزنك نانوي البنية، مما يسمح باتحاد مجموعتي الكربوكسيل و الكحول الفينوليتين الموجودتين في حمض الدبالية مع سطح أكسيد الزنك و تشكيل رابطة قوية بينهما. أضف إلى ما سبق أن أكسيد الزنك النانوي البنية يحرر من سطحه أيونات الزنك الموجبة (كاتيونات الزنك) و التي لها تأثير كبير في تفاقم الترسبات على سطح الغشاء. من الجهة الأخرى، أظهرت الأغشية المصنعة بوجود ثاني أكسيد التيتانيوم نانوي البنية تحسناً ملحوظاً في منع الترسبات من التشكل على سطحها، و ذلك بالمقارنة مع الأغشية البولسلفونية و الأغشية المصنعة بوجود مركب أكسيد الزنك نانوي البنية. و بالرغم من أن نفاذية الأغشية المصنعة بوجود ثاني أكسيد التيتانيوم فاقت الأغشية البوليسلفونية مما يدل على تواجد الحمض بشكل أكبر على السطح. أظهرت النتائج أن الأغشية المصنعة بوجود ثاني أكسيد التيتانيوم لا تتجذب بشكل كبير لحمض الدبالية.

بناء على النتائج السابق ذكرها، فإن الاستنتاج الذي تم التوصل إليه هو أن الأغشية المصنعة باستخدام مركبات نانوية البنية تختلف في طبيعتها الفيزيائية و الكيميائية عن الأغشية المحضرة باستخدام نفس البوليمر. كما أن الاختلاف الفيزيائي و الكيميائي في طبيعة هذه الأغشية المصنعة باستخدام مركبات نانوية البنية تعتمد اعتماداً كبيراً على طبيعة المركب النانوي المستخدم في تحضيرها، و هذا بالتالي يشكل أحد أكبر العوامل في تفاعلها مع المواد الطبيعية المكونة للترسبات مثل حمض الدبالية. لقد أظهرت الأغشية المصنعة باستخدام أكسيد الزنك و ثاني أكسيد التيتانيوم تحسناً كبيراً في نفاذية المياه. الاختلاف في تفاعلها مع حمض الدبالية كان يعزى إلى اختلاف الطبيعة الكيميائية لكلا المركبين.